Article: Discoveries

Faster-X adaptive differentiation under divergence-with-gene-flow in diploids and haplodiploids

Authors: Emily E. Bendall[1,2], Robin Bagley[1,3], Catherine R. Linnen*[1], Vitor C. Sousa[4]*,

Affiliations:

[1] Department of Biology, University of Kentucky, Lexington, Kentucky 40506, USA

[2] Department of Microbiology and Immunology, University of Michigan, Ann Arbor, Michigan 48109, USA

[3] Department of Evolution, Ecology, and Organismal Biology, The Ohio State University at Lima, Lima, OH 45804, USA

[4] CE3C – Centre for Ecology, Evolution and Environmental Changes, Department of Animal Biology, Faculdade de Ciências da Universidade de Lisboa, University of Lisbon, Campo Grande 1749-016 Lisboa, Portugal

*These authors contributed equally. Correspondence: vmsousa@fc.ul.pt; catherine.linnen@uky.edu

Keywords: faster-X, gene flow, divergent selection/adaptation, sex chromosomes, haplodiploids

Abstract

Empirical data from diverse taxa indicate that the hemizygous portions of the genome (X/Z chromosomes) evolve more rapidly than their diploid counterparts. Faster-X theory predicts increased rates of adaptive substitutions between isolated species, yet little is known about species experiencing gene flow. Here we investigate how hemizygosity impacts genome-wide patterns of differentiation during adaptive divergence with gene flow, combining simulations under isolation-with-migration models, a meta-analysis of autosomes and sex-chromosomes from diverse taxa, and analysis of haplodiploid species. First, using deterministic and stochastic simulations, we show that elevated differentiation at hemizygous loci occurs when there is gene flow, irrespective of dominance. This faster-X adaptive differentiation stems from more efficient selection resulting in reduced probability of losing the beneficial allele, greater migration-selection threshold, greater allele frequency differences at equilibrium, and a faster time to equilibrium. Second, by simulating neutral variation linked to selected loci, we show that faster-X differentiation affects linked variation due to reduced opportunities for recombination between locally adaptive and maladaptive immigrant haplotypes. Third, after correcting for expected differences in effective population size, we find that most taxon pairs (24 out of 28) exhibit faster-X differentiation in the meta-analysis. Finally, using a novel approach combining demographic modeling and simulations, we found evidence for faster-X differentiation in haplodiploid pine-feeding hymenopteran species adapted to different host plants. Together, our results indicate that divergent selection with gene flow can lead to higher differentiation at selected and linked variation in hemizygous loci (i.e., faster-X adaptive differentiation), both in X/Z-chromosomes and haplodiploid species.

Introduction

Widespread empirical patterns provide key insights into underlying evolutionary processes. One of the most common patterns observed in nature is that sex chromosomes (X or Z) behave differently than autosomes as populations and species diverge. Compared to autosomes, sex chromosomes tend to have higher levels of genetic differentiation between populations, greater divergence between species, and higher rates of adaptive substitution, patterns collectively referred to as faster-X evolution (Charlesworth et al. 1987; Martin et al. 2013; Meisel and Connallon 2013; Irwin 2018; Presgraves 2018). However, faster-X evolution is not uniform across taxa (Mank et al. 2010; Presgraves 2018) and need not be attributable to the same underlying evolutionary causes (Lasne et al. 2017). A key challenge for evolutionary theory, therefore, is to comprehensively characterize conditions that impact the presence and magnitude of faster-X evolution. Additionally, to draw accurate inferences from a growing deluge of genome-wide divergence and differentiation datasets, the impact of sex-linkage needs to be considered alongside other factors that give rise to heterogeneous genetic differentiation across the genome (Seehausen et al. 2014; Ravinet et al. 2017; Wolf and Ellegren 2017).

Population genetics theory generates many predictions regarding how hemizygosity—the presence of a single functional copy of X- and Z- chromosomes in males and females, respectively—affects the evolution of sex-linked alleles relative to otherwise equivalent autosomal alleles. Because new recessive or partially recessive mutations on the X (or Z) chromosome are immediately exposed to selection in the heterogametic sex, such mutations will be fixed by positive selection or purged by purifying selection more rapidly compared to recessive autosomal mutations (Avery 1984; Charlesworth et al. 1987; Hedrick and Parker 1997). More efficient selection on novel hemizygous alleles will also impact linked variation via hitchhiking (Betancourt et al. 2004) and background selection (Charlesworth 2012). However, if adaptation proceeds via standing genetic variation instead of new mutations (Hermisson and Pennings 2005; Barrett and Schluter 2008) beneficial mutations will fix more rapidly on diploid autosomes, regardless of dominance (Charlesworth et al. 1987; Orr and Betancourt 2001; Connallon et al. 2012; Meisel and Connallon 2013) because autosomes tend to harbor more genetic diversity than sex chromosomes due to larger effective size. Based on this theoretical work, one possible explanation for the observation that adaptive substitution rates on sex

chromosomes tend to outpace those on the autosomes is that adaptation is driven primarily by new, partially recessive mutations (Presgraves 2018, but see Wright et al. 2015).

Another factor that is expected to differentially impact substitution rates on sex chromosomes versus autosomes is a difference in copy number that results in different effective population sizes (N_e). Assuming a 50:50 sex ratio and equal fitness variances for males and females, the N_e of X or Z chromosomes is ¾ that of autosomes. The reduced N_e of sex chromosomes should increase the fixation rate of neutral mutations by genetic drift (Wright 1931). A smaller N_e will also decrease the efficacy of selection on sex chromosomes, enabling more mildly deleterious alleles to escape purifying selection and slowing the rate of adaptive substitution (Kimura and Ohta 1971; Ohta 1973; Orr and Betancourt 2001; Betancourt et al. 2004). Moreover, a smaller N_e will also result in lower scaled recombination ($2N_er$) and migration ($2N_em$) rates, assuming that recombination rate r and migration rate m are identical across the genome. For these reasons, demographic factors that modify the ratio of sex-chromosome N_e to autosome N_e (e.g., biased sex ratios or a high variance in reproductive success in one sex) can either restrict or broaden the conditions under which faster-X evolution will occur (Vicoso and Charlesworth 2009). Consistent with this prediction, differences in the magnitude of faster-X evolution across diverse animal taxa correlate with differences in overall N_e and in demographic characteristics that affect the X (or Z) N_e to autosome N_e ratio. Although differences in dosage compensation mechanisms, which impact the relative fitness of the heterogametic sex (Charlesworth et al. 1987), may also be important (Mank et al. 2010).

Despite considerable theoretical and empirical progress, several gaps in our understanding of faster-X evolution remain. First, most theoretical work to date has focused on how hemizygosity impacts the accumulation of fixed genetic differences between isolated populations or species. By comparison, much less is known about how faster-X evolution impacts genetic differentiation as populations diverge in the face of gene flow (but see (Owen 1986; Nagylaki 1996; Parker and Hedrick 2000; Höllinger and Hermisson 2017; Lasne et al. 2017), a common scenario in natural populations (reviewed in Feder et al. 2012; Sousa and Hey 2013; Seehausen et al. 2014; Tigano and Friesen 2016). When populations diverge in the absence of gene flow, the main mechanism through which hemizygosity will impact differentiation levels at divergently selected loci is via reducing the loss of low-frequency, recessive alleles to drift

(increased efficacy of selection against drift). However, when populations are connected by gene flow, hemizygosity can also impact differentiation levels via increasing the efficacy of selection against maladapted, migrant alleles (increased efficacy of selection against migration).

One of the few studies that has examined faster-X evolution in the context of divergence-with-gene-flow modeled a scenario in which divergently selected populations are connected by gene flow and alternative alleles at the selected locus are both common, with an initial frequency of 0.5 (Lasne et al. 2017). Under strong migration ($m>>s$), these deterministic models predict that the magnitude of faster-X differentiation depends mostly on sex-specific migration and appears to be insensitive to dominance, effective population size, and sex-biased selection (Lasne et al. 2017). This contrasts with models without migration that predict faster-X divergence only when mutations are recessive. These results suggest that the mechanisms underlying faster-X divergence in isolated populations differ in kind from the mechanisms that give rise to faster-X differentiation in populations connected by gene flow. However, this conclusion rests on the assumptions of strong migration and that local adaptation is largely attributable to standing genetic variation segregating at intermediate allele frequencies. While there is little doubt that standing genetic variation is an important source of adaptive genetic variation (Messer and Petrov 2013), there are also abundant examples of adaptation from new or low-frequency variants (Linnen et al. 2009; Karasov et al. 2010; Peter et al. 2012; Pfenninger et al. 2015). Additionally, scenarios involving local adaptation with weaker migration are also likely to be common in nature (Pinho and Hey 2010; Hey and Pinho 2012; Tigano and Friesen 2016).

Another gap in our understanding of faster-X evolution in divergence-with-gene-flow scenarios is how hemizygosity impacts differentiation at loci that are physically linked to sites under divergent selection. Because the effects of selection on linked neutral variation depend on recombination, patterns of differentiation on hemizygous chromosomes are likely to differ from diploid autosomes simply because hemizygous chromosomes do not recombine in one of the sexes (Lester and Selander 1979; Owen 1988; Betancourt et al. 2004). Furthermore, in the absence of migration, theory predicts faster fixation of beneficial alleles located on hemizygous chromosomes (Avery 1984), reducing opportunities for linked neutral alleles to recombine away from the selected locus (Owen 1988; Betancourt et al. 2004). To date, several theoretical studies have explored how gene flow under different demographic histories, selection regimes, and

genome features affect genetic variants linked to locally maladapted immigrant loci, ultimately shaping genome-wide patterns of genetic differentiation (Petry 1983; Barton and Bengtsson 1986; Charlesworth et al. 1997; Feder and Nosil 2010; Jeffrey L. Feder et al. 2012; Cruickshank and Hahn 2014; Yeaman et al. 2016; Aeschbacher et al. 2017; Ravinet et al. 2017; Matthey-Doret and Whitlock 2019). However, hemizygosity has been largely ignored in this context, and the few studies that have addressed the effects of linked selection at hemizygous loci with migration focused on scenarios of secondary contact between fully differentiated species, investigating the impact of incompatibilities (Fusco and Uyenoyama 2011; Muirhead and Presgraves 2016; Fraïsse and Sachdeva 2021). To our knowledge, the effects of linked selection at hemizygous loci have not been examined under scenarios of divergence with gene flow driven by divergent selection. Such analyses are essential to identify conditions that could lead to chromosome-wide faster-X differentiation due to divergent selection and local adaptation. Regardless of the divergence scenario, a key challenge for empirical data is to distinguish between faster-X adaptive differentiation, which we define here as elevated differentiation due to the interaction between hemizygosity and positive selection, and faster-X differentiation due to other processes, such as increased differentiation due to drift.

A final gap in faster-X research is a lack of studies investigating haplodiploid organisms, which together account for an estimated 15% of all animal species (Hedrick and Parker 1997). Haplodiploidy is a genetic system in which females develop from fertilized eggs and are diploid, whereas males are haploid either because they develop from unfertilized eggs (arrhenotokous haplodiploidy) or because they undergo paternal genome elimination after fertilization (Normark 2003). Because males are haploid and females are diploid, the entire genomes of haplodiploid organisms are, in some respects, analogous to X (or Z) chromosomes in diploid organisms. Thus, if hemizygous selection is largely responsible for faster-X evolution in diploid sex chromosomes, this same mechanism should give rise to faster evolution in entire haplodiploid genomes compared to comparable diploid autosomes (Hedrick and Parker 1997). Alternatively, if the predominant mechanisms underlying elevated divergence and differentiation on sex chromosomes are unique to sex chromosomes (e.g., increased susceptibility to recurrent bouts of meiotic drive (Frank 1991; Hurst and Pomiankowski 1991; Meiklejohn et al. 2018; Patten 2018) or rapid divergence in sex chromosome regulation (Lifschytz and Lindsley 1972; Campbell et al. 2013)), then haplodiploids may not exhibit accelerated rates of evolution relative to diploids.

Thus, haplodiploids provide an opportunity to disentangle the effects of sex-chromosome-specific factors and hemizygosity on evolutionary rates.

Despite their potential, haplodiploids have not been widely used to investigate faster-X evolution (but see Hedrick and Parker 1997), likely because they lack a built-in benchmark for estimating the magnitude of faster-X evolution. In diploid organisms, differentiation levels and substitution rates for X- and Z-chromosomes can be compared to their autosomal counterparts from the same taxa, thereby controlling for lineage-specific traits and historical factors that impact baseline levels of genetic variation. For haplodiploid organisms, the only benchmarking option currently available is to make comparisons to ecologically and demographically similar diploid organisms, which are likely separated by millions of years of independent evolution. Fortunately, new tools for simulating genomic variation under a variety of demographic and selection scenarios (Hoban et al. 2012; Haller and Messer 2019) offer an alternative benchmarking strategy: simulate diploid analogs to observed haplodiploid data. However, this strategy has not, to our knowledge, been used.

Here, we extend previous work on faster-X evolution in several ways. First, using a combination of deterministic and stochastic simulations of adaptive divergence-with-gene-flow, we characterize conditions that will lead to elevated differentiation at hemizygous loci (i.e., those located on X chromosomes, Z chromosomes, and within haplodiploid genomes) relative to diploid loci. Overall, we find that hemizygosity increases differentiation at selected sites via increasing the efficacy of selection against both drift and migration and that faster-X differentiation occurs for both recessive and codominant alleles. Second, to connect our simulations to empirical datasets, we also simulate neutral variation linked to divergently selected sites. Faster-X differentiation at linked neutral sites is caused by reduced opportunities for recombination between locally adaptive and maladaptive haplotypes and is most pronounced when selection is strong, alleles are recessive, and migration rates are high. Third, based on these simulations, we devise strategies for identifying faster-X adaptive differentiation in genomic datasets and apply these to (1) a meta-analysis of sex chromosome vs. autosome differentiation, and (2) a pair of haplodiploid sister species that have undergone divergence-with-gene-flow. Overall, we find evidence for widespread faster-X adaptive differentiation in nature and highlight priorities for future theoretical and empirical work.

Results and Discussion

Faster-X differentiation under divergence-with-gene-flow

To investigate how the evolutionary dynamics of hemizygous chromosomes differ from those of diploid chromosomes, we consider a scenario that is likely to be common in nature: colonization of a new geographic area with open niches that generate divergent natural selection on habitat-related traits, with continued exchange of migrants as populations diverge (e.g., Lamichhaney et al. 2015; Samuk et al. 2017; Malinsky et al. 2018). To model this scenario, we simulate a single locus in two populations that are adapting to different niches while experiencing symmetric migration, with alleles *a* and *A* favored in populations 1 and 2, respectively (Figure 1). We then compare outcomes for diploid and hemizygous loci. To gain greater insight into the evolutionary processes that give rise to faster-X differentiation, we explore this scenario via a series of simulations of increasing complexity across many parameter combinations (Supplementary Table S1). In the following, we use the term faster-X differentiation for simplicity, but note that it corresponds to faster-X adaptive differentiation since we modeled a scenario with divergent selection. First, we use deterministic simulations to examine migration-selection dynamics in the absence of genetic drift. With these simulations, we examine not only how hemizygosity impacts equilibrium F_{ST} values at a divergently selected locus (Lasne et al. 2017), but also how hemizygosity impacts the time to equilibrium and the migration threshold for a new beneficial allele (Yeaman and Otto 2011). Second, we use stochastic simulations to examine how hemizygosity impacts differentiation levels when there is genetic drift in addition to migration and selection. We use these simulations to explore differentiation (1) at the selected locus only and (2) at linked neutral sites. To tease apart the opposing effects of hemizgyosity and reduced effective population size, we perform the stochastic simulations with and without a scaling correction (see Material and Methods). In all simulations, faster-X differentiation was measured as the ratio of F_{ST} at a hemizygous locus to F_{ST} at a comparable diploid locus. Throughout, we ask how selection strength, migration rate, dominance, and starting allele frequency impact the magnitude of faster-X differentiation.

Deterministic simulations: selection-migration dynamics at selected locus

We used deterministic simulations to explore three potential mechanisms through which hemizygous selection can give rise to faster-X differentiation. Specifically, we ask: (1) How does hemizygosity impact the migration threshold for a new, beneficial allele?, (2) How does hemizygosity impact the time it takes to reach migration-selection equilibrium?, and (3) How does hemizygosity impact equilibrium differentiation levels?

Migration threshold for a new mutation

When a population colonizes a novel niche and continues to receive migrants from another habitat, new or low-frequency autosomal mutations that are beneficial in the new habitat may never gain a foothold, especially if they are recessive and invisible to selection in heterozygotes. By exposing recessive alleles to selection, hemizygosity is likely to increase the chances that a novel recessive allele escapes swamping by gene flow. To evaluate this prediction, we compared the migration threshold for "new" ($q_0 = 10^{-5}$) alleles on hemizygous chromosomes versus diploid chromosomes. As expected, we found that for a given selection coefficient, hemizygous loci with new or very low frequency recessive mutations that were beneficial in population 1 could always diverge at higher migration rates than comparable diploid loci (Figure 2A). The region of parameter space where divergence occurred at hemizygous loci but not diploid loci was primarily when $s<m$. However, differences in migration thresholds between hemizygous and diploid loci disappeared when the new mutation was codominant (Figure 2B). We also found that our diploid simulation results fit Yeaman and Otto (2011)'s analytical approximation reasonably well (Figure 2). All else equal, these results suggest that there will be a disproportionate contribution of hemizygous loci to local adaptation when gene flow is high and adaptation is driven by new recessive mutations.

Time to migration-selection equilibrium

Assuming that adaptation to a novel habitat proceeds via standing genetic variation instead of new mutations and selection is sufficiently strong relative to migration, differentiation at the selected locus will increase over time until a balance is reached between divergent selection and homogenizing gene flow. But the time that it takes to reach this equilibrium might depend on starting allele frequencies, dominance, selection strength, and the rate of gene flow

(Charlesworth et al. 1997; Betancourt et al. 2004). By increasing the efficacy of selection, hemizygous loci are likely to reach equilibrium differentiation levels faster than diploid loci, which is predicted by models without migration (Avery 1984; Betancourt et al. 2004). To evaluate whether this prediction holds when there is migration, we determined for each set of parameters the number of generations it took to reach equilibrium.

After 100,000 generations, many deterministic simulations had not yet reached migration-selection equilibrium, especially when migration was stronger than selection ($m>s$). Diploid loci failed to reach equilibrium under a wider range of parameter combinations than hemizygous loci (Supplementary Figure S1). Considering only those areas of parameter space for which equilibrium was reached for at least one type of locus, hemizygous loci always reached equilibrium at the same rate or faster than diploid loci (Supplementary Figures S2 and S3). Differences in the time to equilibrium were maximized when: (1) the starting minor allele frequency was low (i.e., further from equilibrium allele frequency); and (2) the minor allele was recessive. Overall, these results demonstrate that the increased efficacy of selection on hemizygous loci can have a substantial impact on the time it takes populations to reach equilibrium differentiation levels.

Differences in the time to equilibrium predict that populations will start to exhibit appreciable differentiation at hemizygous loci long before differentiation will occur at comparable diploid loci, shown by the allele trajectories in the diverging populations (Supplementary Figure S3). If populations are sampled before they reach equilibrium, differences in allele trajectories can translate into substantially higher differentiation at hemizygous loci relative to the diploid loci, especially if the derived allele is recessive and started at a low frequency. These differences in allele frequency trajectories can also impact linked variation (Owen 1988; Betancourt et al. 2004; see below).

Migration-selection equilibrium differentiation levels

Under a deterministic model, populations will eventually reach migration-selection equilibrium regardless of starting allele frequency (Supplementary Figure S3). In the absence of migration, fixation of different alleles in the two populations eventually occurs for both diploid and hemizygous loci. However, with migration, the increased efficacy of selection on hemizygous loci compared to diploid loci should result in concomitant increases in equilibrium

levels of differentiation. To test this prediction, we compared equilibrium F_{ST} values within the subset of parameter space of strong selection relative to migration ($s>m$) and for which both hemizygous and diploid loci reached equilibrium. As predicted, F_{ST} values at hemizygous loci were higher than at diploid loci under large regions of parameter space, consistent with faster-X differentiation (Figure 3). Interestingly, we observed faster-X differentiation for both recessive and codominant alleles. Although the region of parameter space that gives rise to faster-X differentiation was wider in the recessive case, the magnitude of the faster-X effect was greater for the codominant case under some parameter combinations (Figure 3, Supplementary Figure S4). This is explained by the asymmetry in the equilibrium allele frequencies between populations for the recessive case with migration (Figure 3B). Overall, these results demonstrate that even after migration-selection equilibrium has been reached, the increased efficacy of selection on hemizygous chromosomes can produce faster-X differentiation that will persist so long as conditions remain stable. In contrast to differences in the migration threshold, faster-X differentiation stemming from differences in equilibrium differentiation levels occurs even in the case of codominance.

Stochastic simulations: drift-selection-migration dynamics at selected locus and linked neutral sites

To explore how hemizygosity impacts differentiation at both selected loci and linked neutral sites when there is drift and migration, we performed stochastic simulations using the forward framework implemented in SLiM3. To tease apart the effects of hemizygous selection and effective size, we performed two types of simulations: "unscaled" in which the hemizygous chromosomes have ¾ of the N_e of diploid chromosomes; and "scaled" in which hemizygous chromosomes and diploid chromosomes experience equivalent effective levels of drift, migration, and recombination. We focused on three specific questions: (1) How does the increased efficacy of selection on hemizygous loci impact differentiation at the selected site when there is selection, migration, and drift?, (2) How does hemizygosity impact differentiation at linked neutral sites?, and (3) To what extent do differences in effective size between hemizygous chromosomes and diploid chromosomes impact faster-X differentiation?

Faster-X differentiation at the selected locus

When populations evolve under divergent selection, genetic drift and gene flow, the increased efficacy of selection on hemizygous loci can increase differentiation relative to diploid loci via two routes. First, the increased efficacy of selection against drift will increase the probability that a beneficial allele at a hemizygous locus will escape loss via drift relative to a comparable diploid locus, especially if the allele is recessive and rare. Second, even when we ignore differential rates of allele loss, the differences in the efficacy of selection against migration can result in higher levels of differentiation on hemizygous loci. To evaluate the contribution of these two mechanisms to faster-X differentiation in the absence of differences in effective population size, we focused on the "scaled" simulations (see "*Impact of reduced effective size*" for unscaled comparisons). We computed the average F_{ST} at the selected site for each parameter combination in two ways (Figure 1C): using all 1000 simulations and using only those simulations that retained the derived allele *a* favored in population 1. By averaging F_{ST} across all simulations, we estimate the total impact of hemizygosity on differentiation levels via all mechanisms. By conditioning on retaining the derived allele, we isolate the effect of hemizygosity on selection *vs*. migration.

Comparing F_{ST} ratios estimated from all simulations (Figure 4A) to F_{ST} ratios that were conditioned on maintaining variation at the selected locus (Figure 4B), it is clear that hemizygosity gave rise to faster-X differentiation at the selected site via increased efficacy against drift. Also, as predicted, the impact of differential allele loss on faster-X differentiation was most pronounced for alleles that were recessive (note large difference between Figure 4A vs. 4B for recessive alleles in comparison to codominant alleles) and rare (differences between Figure 4A and 4B decreased as q_0 increased). Without migration ($2Nm$=0), average F_{ST} ratios across selection coefficients ranged from 1.00 to 4.30 for recessive alleles and from 1.00 to 1.72 for codominant alleles, whereas with migration ($2Nm$>0.5) these ratios ranged from 1.00 to 4.68 for recessive alleles and from 1.00 to 2.00 for codominant alleles (Supplementary Table S2).

To evaluate the hypothesis that an increased probability of allele retention contributes to faster-X differentiation, we calculated the proportion of simulations for which the derived allele was retained for each parameter combination. As expected, hemizygous loci had a higher probability of retaining the derived allele across a wide range of parameter combinations

(Supplementary Figure S5). For recessive alleles, differences in allele retention between hemizygous and diploid loci were dependent on both starting allele frequency and selection strength, but insensitive to migration rate. By contrast, differences in allele retention between hemizygous and diploid loci were minimal for the codominant case. The limited impact of migration rate on retention probability is consistent with the dynamics at this phase being mostly driven by genetic drift and selection, which is a common simplification of models with gene flow (e.g., Yeaman et al. 2016).

Consistent with our deterministic simulation results, we observed faster-X differentiation at the selected locus even after conditioning on allele retention (Figure 4B). Although these simulations included drift, faster-X differentiation patterns at the selected locus were relatively insensitive to initial allele frequency, indicating that once the favored allele escaped loss due to drift these dynamics were driven primarily by selection and migration. Overall, stochastic simulations recapitulated several key results observed in our deterministic simulations, including: (1) faster-X differentiation was maximized when migration was high ($2N_em>0.5$) and selection was moderate ($10<2N_es<40$), (2) faster-X differentiation was observed for both recessive and co-dominant alleles, and (3) while more parameter combinations gave rise to faster-X differentiation in the recessive case, the magnitude of faster-X differentiation was greater in the codominant case when there was high migration ($2Nm=5$) and moderate selection ($10<2Ns<20$).

In the stochastic simulations, we also observed the same mechanisms that gave rise to faster-X differentiation in the deterministic simulations. First, the probability of reaching "equilibrium" differentiation levels was higher for hemizygous loci, particularly in regions of parameter space for which we observed greater faster-X differentiation (Supplementary Figure S6). Second, hemizygous loci took less time to reach equilibrium differentiation than diploid loci, especially in the recessive case (Supplementary Figure S7). And third, allele frequency trajectories from the stochastic simulations recapitulated patterns observed in the deterministic simulations (Figure 3). Taken together, our results demonstrate that hemizygosity gives rise to faster-X differentiation at the selected site via both increased allele retention and increased efficacy at removing maladapted migrant alleles. The impact of drift on faster-X differentiation is most pronounced when the selected allele is rare and recessive, but faster-X differentiation

stemming from the increased efficacy of selection against migration occurs regardless of dominance and initial allele frequency.

Faster-X differentiation at linked neutral sites

When we computed weighted F_{ST} across 500-kb genomic regions surrounding the selected site, we saw several striking differences (Figure 4 vs. Figure 5). For example, compared to the selected site, differential allele loss had less impact on faster-X differentiation at linked sites. Specifically, while faster-X differentiation patterns at linked sites differed somewhat between conditioned (Figure 5B) and non-conditioned (Figure 5A) results—especially in the recessive, low-frequency cases—these differences were far less pronounced than those observed at the selected sites (Figure 4B *vs* Figure 4A). For linked neutral sites, the average hemizygous/diploid ratios of F_{ST} (500-Kb window) for non-conditioned results ranged from 0.99 to 2.55 for the recessive case and 0.99 to 1.25 for the codominant case; when results were conditioned on allele retention, F_{ST} ratios ranged from 0.83 to 1.44 for the recessive case and 0.88 to 1.24 for the codominant case (Supplemental Table S3).

Conditioning on allele retention revealed both similarities and differences in the manner in which the increased efficacy of selection against migration gives rise to faster-X differentiation at the selected site (Figure 4B) and at linked sites (Figure 5B). Faster-X differentiation for both selected and linked sites was maximized when migration was high ($2Nm$=5) and was relatively insensitive to minor allele frequency. However, compared to selected sites, faster-X differentiation at linked neutral sites responded very differently to both selection strength and dominance. First, faster-X differentiation at linked sites was always maximized at higher selection coefficients ($2N_es$>30) than at the selected site (maximized at $2N_es$~10). Second, whereas dominance did not appear to impact the efficacy of selection against migration for the selected site (Figure 4B), faster-X differentiation was much more pronounced at linked sites when the selected site was recessive (Figure 5B).

Differences in patterns of faster-X differentiation between selected and linked neutral sites reflect the action of recombination. The specific patterns depended on how much opportunity there was for recombination between locally adaptive and maladaptive immigrant haplotypes, allowing for an immigrant neutral allele linked to the maladapted allele to recombine into the favored haplotype. The smaller the opportunity for recombination in hemizygous

chromosomes relative to diploid chromosomes, the greater the magnitude of faster-X differentiation at linked neutral sites. As populations diverge, hemizygosity can reduce recombination between divergently selected haplotypes in three ways. First, for a given haplotype frequency, the proportion of the population that is heterozygous for immigrant and local haplotypes will always be lower in the hemizygous case than in the diploid case simply because hemizygous individuals cannot be heterozygous. Second, once diverging populations reach migration-drift-selection equilibrium, the higher allele frequency differences at selected site in hemizygous loci decreases the proportion of heterozygotes in one or both populations. Third, the increased efficacy of selection on hemizygous loci could reduce opportunities for recombination between divergently selected haplotypes by decreasing the time it takes diverging populations to reach equilibrium.

To examine how opportunities for recombination impacted faster-X differentiation at linked sites, we considered the scaled simulations and examined F_{ST} ratios alongside allele frequency trajectories and genome scans of F_{ST} (Figure 6). At lower selection coefficients ($2Ns$=10), where faster-X differentiation was maximized at selected sites but not at linked sites, F_{ST} at linked sites dropped off quickly to the expected neutral F_{ST} for both hemizygous and diploid chromosomes (Figure 6B). The allele trajectories revealed that the narrow windows of differentiation surrounding the selected site were likely caused by increased opportunities for recombination due to substantial numbers of immigrant (maladapted) haplotypes in each population. These patterns were unaffected by dominance. By contrast, at higher selection coefficients ($2Ns$=200), faster-X differentiation was maximized at linked sites but not at the selected site. Under these conditions, F_{ST} was elevated well outside of the selected site for hemizygous chromosomes, but less so for diploid chromosomes (Figure 6C). Additionally, the difference between the hemizygous and diploid chromosomes was greatest when the derived allele was recessive. In that case, diploid chromosomes harbored more locally maladaptive *a* alleles in population 2 at equilibrium since they are hidden from selection in heterozygotes, thereby providing more opportunity for recombination between divergently selected haplotypes, reducing differentiation at linked sites. Hemizygous loci also reached equilibrium more quickly (Supplementary Figure S7). When the derived allele was codominant, the equilibrium allele frequencies were similar for both hemizygous and diploid loci, but hemizygous loci reached equilibrium slightly more quickly than diploid loci. Compared to the recessive case, the

difference in time to equilibrium was much smaller. Thus, faster-X differentiation at linked sites is reduced under codominance because hemizygous and diploid chromosomes have similar opportunities for recombination.

To explore how recombination rate impacts faster-X differentiation at linked sites, we repeated the simulations with linked variation under a lower recombination rate for two starting allele frequencies (q_0= 0.10, 0.50). Reducing the recombination rate caused faster-X differentiation at linked sites to resemble faster-X differentiation at selected sites (Supplemental Figure S8). For example, reducing the recombination rate increased the contribution of allele loss to faster-X differentiation at linked sites. Additionally, regions of parameter space maximizing faster-X differentiation shifted towards lower selection coefficients.

Overall, our linked selection simulations demonstrate that hemizgyosity can have a substantial impact on differentiation levels at neutral sites linked to loci that experience divergent natural selection, especially if migration rates are higher than $2Nm$=0.5. Our results also suggest that faster-X differentiation at linked sites is largely attributable to differences in the efficacy of selection against migrant alleles rather than differences in the efficacy of selection against drift, although the latter increases in importance as recombination rates decline. This insensitivity to drift explains why faster-X differentiation at linked sites is insensitive to starting allele frequencies. Finally, as was the case for selected sites, faster-X differentiation at linked sites can occur even in the case of codominance when there is gene flow.

Impact of reduced effective size

When comparing autosomes with X or Z chromosomes, differences in effective sizes can affect differentiation patterns. In particular, reduced effective population sizes for hemizygous chromosomes should reduce the efficacy of selection, potentially dampening the observed effects on differential allele retention and resistance to gene flow. However, our unscaled simulations, in which X (or Z) chromosomes had 3/4 of the effective size of autosomes, revealed that differences in effective population size had very little impact on faster-X differentiation at the selected site (Supplementary Figure S9). This was true both for the results that included the impact of differential allele loss (Supplementary Figure S9A) and for the results conditioned on allele retention (Supplementary Figure S9B). The main difference for the selected site was that the unscaled simulations produced faster-X differentiation in regions of parameter space with

lower migration rates and lower selection coefficients (Figure 4 *vs*. Supplementary Figure S9). This difference is due to increased neutral differentiation in the hemizgyous chromosomes. By contrast, when we examined unscaled results for linked neutral sites, we observed a dramatic increase in faster-X differentiation across all regions of parameter space due to increased drift (Supplementary Figure S10, Supplementary Tables S4-S5).

Together, our unscaled analyses revealed that rather than dampening the increased efficacy of selection, the reduced effective size of hemizygous chromosomes increased faster-X differentiation due to drift and lower scaled migration. Furthermore, the strong impact of reduced effective size on faster-X differentiation at linked sites is likely to complicate the detection of selection on hemizygous chromosomes, a common goal of empirical population genomic studies. We therefore evaluated two potential corrections for this effect. First, we adjusted autosomal F_{ST} values by a factor f_{XA}=4/3 given that the X (or Z) hemizygous chromosome have 3/4 of the effective size of diploid autosomes with a 50:50 sex ratio (see details in Material and Methods). Comparing the adjusted F_{ST} values (Supplementary Figure S11) to the scaled analyses (Figure 5) revealed that the adjustment identifies regions of elevated differentiation due to selection. We use this adjustment for the empirical meta-analysis (see "*Empirical data: Meta-analysis of sex chromosomes vs. autosomes*").

We also evaluated a second adjustment strategy dividing the hemizygous and diploid F_{ST} by the corresponding neutral values for a given migration rate. The resulting corrected faster-X differentiation (Supplementary Figure S12) was nearly identical to that observed for the scaled analyses (Figure 5). For real data, one way to approximate the neutral F_{ST} for a given migration rate would be to use the observed F_{ST} at regions of the genome that are unlikely to be impacted by selection, such as intergenic regions (Gronau et al. 2011) or regions with high recombination (Pouyet et al. 2018). Overall, these results suggest that if faster-X differentiation persists even after correcting for reduced effective size, this differentiation could be attributable to differences in the efficacy of selection on hemizygous chromosomes relative to diploid chromosomes.

Simulation results: implications for faster-X theory and limitations

Overall, our simulations demonstrate multiple mechanisms through which increased efficacy of selection on hemizygous chromosomes can give rise to faster-X adaptive differentiation when there is divergent selection with gene flow. Considering the selected site

only, hemizygous loci have higher migration thresholds (Figure 2), are less likely to lose rare alleles to drift (Suplementary Figure S5), reach equilibrium differentiation levels faster (Suplementary Figures S2 and S7), and have higher equilibrium differentiation levels compared to otherwise equivalent diploid loci (Figures 3-4). These differences are minimally impacted by a reduced effective population size for hemizygous chromosomes (Suplementary Figure S9-S12). We can group the observed faster-X differentiation mechanisms into three distinct phases. In the first phase, the dynamics of a divergently selected, low-frequency allele is mostly determined by the risk of loss due to drift (Figure 4, Supplementary Figure S5). The increased efficacy of selection against drift and the reduced probability of allele loss at hemizygous loci in a divergence-with-gene-flow scenario is analogous to classical faster-X divergence among isolated populations in which dominance has a large impact on the outcomes (e.g. Charlesworth et al. 1987; Vicoso and Charlesworth 2009b; Meisel and Connallon 2013; Charlesworth et al. 2018). Once populations escape phase 1 without losing the divergently selected allele, there is a second transitional phase during which the increased efficacy of selection against locally maladaptive alleles causes hemizygous loci to differentiate more rapidly than comparable diploid loci. Again, this is in line with classical faster-X theory demonstrating shorter sojourn times for beneficial X-linked alleles in isolated populations (Avery 1984; Betancourt et al. 2004). During phase 2, differences in times to equilibrium occur regardless of dominance, but differences are far greater for recessive alleles (Supplementary Figure S7).

Once diverging populations approach equilibrium between selection, migration, and drift, they enter phase 3. In this phase, hemizygosity increases the efficacy of selection against locally maladapted immigrant alleles, resulting in higher allele frequency differences at hemizygous loci compared to diploid loci (Figures 4 and 6). Consistent with deterministic results obtained under a similar divergence model that assumed strong migration ($m>>s$; Lasne et al. 2017), we find that when populations remain connected by gene flow, faster-X differentiation occurs irrespective of dominance, even when selection is stronger than migration ($s>m$). Moreover, in some regions of parameter space, the magnitude of faster-X differentiation is greater in the codominant case (Figures 3-4). These findings contrast with classical faster-X theory that has been developed for divergence in isolation, which predicts increased substitution rate only when beneficial mutations are recessive (e.g. Charlesworth et al. 1987; Vicoso and Charlesworth 2006; Meisel and

Connallon 2013; Charlesworth et al. 2018) or when codominance is accompanied by deviations from 50:50 sex ratio (Vicoso and Charlesworth 2009).

We also build on previous faster-X differentiation theory by evaluating the effect of hemizygous selection on linked neutral sites under a divergence-with-gene-flow scenario. In contrast to the selected site, the reduced probability of losing beneficial alleles to drift at hemizygous loci (phase 1) has minimal impact on differentiation at linked neutral sites, assuming sufficient recombination (Figure 5). Instead, faster-X adaptive differentiation at linked neutral sites occurs primarily during phases 2 and 3, when hemizygosity reduces opportunities for recombination between locally adaptive and maladaptive haplotypes, even in scaled simulations with identical recombination rates (Figure 6). In phase 2, hemizygous loci differentiate more rapidly (Supplementary Figure S7) affecting linked variation (Figures 5-6), analogous to the impact of reduced sojourn times on X-linked variation in isolated populations (Owen 1988; Betancourt et al. 2004). In phase 3, efficient selection against maladapted migrant alleles causes reduced opportunities for recombination. This mechanism produces faster-X differentiation at neutral sites linked to both recessive and codominant alleles, with faster-X differentiation most pronounced in the recessive case (Figure 5B). These results are also consistent with predictions from deterministic continent-island models of secondary-contact (Fusco and Uyenoyama 2011; Muirhead and Presgraves 2016; Fraïsse and Sachdeva 2021). Despite several important differences between our model and these secondary contact models, including divergence scenario, migration direction, and the presence of drift, we reach qualitatively similar conclusions. These similarities suggest that in the long term, after migration-selection-drift equilibrium is reached, the impact of the initial phases is negligible.

Overall, our results suggest that the magnitude of faster-X adaptive differentiation in genomic datasets will depend not only on dominance, migration rate, selection strength, and recombination rate, but also on the amount of time that has elapsed since populations began diverging. At the earliest stages of divergence, faster-X differentiation will be confined to selected sites, with dynamics mostly determined by the interaction between selection and drift. Next, as beneficial alleles increase in frequency, there will be an ephemeral phase in which hemizygous loci can exhibit markedly higher differentiation than diploid loci at selected and linked sites due to the combined effects of faster differentiation and hitchhiking. Finally, once

populations approach equilibrium between drift, selection, migration, and recombination, the magnitude of faster-X differentiation at selected and linked sites will stabilize. At this point, our results suggest that faster-X differentiation in genomic datasets can be maintained so long as gene flow between diverging populations or species remains constant.

The proportion of the genome that will exhibit faster-X adaptive differentiation depends on the genetic architecture of adaptation to divergent habitats. Nevertheless, with strong selection and high migration, our results indicate that differentiation windows in hemizygous chromosomes will be wider than in diploid chromosomes and that divergent selection at a single hemizygous locus can reduce gene flow relative to the diploid case even at neutral sites 250 Kb away, corresponding to ~4.40 cM (Figures 5-6). Moreover, the continent-island model of Fusco and Uyenoyama (2011) and Muirhead and Presgraves (2016) predict that selection at hemizygous sites can also impact unlinked neutral markers. Assuming that at equilibrium, adaptive divergence-with-gene-flow dynamics can be reasonably well approximated by the continent-island model, we speculate that localized reductions in gene flow surrounding hemizygous loci could extend to the chromosome-wide level.

Our model makes several simplifying assumptions that could impact faster-X differentiation at selected and linked sites. Relaxing these assumptions and creating more complex, but realistic, models are therefore potentially fruitful avenues for future research. First, the genetic architecture of adaptation to novel niches is likely much more complex (i.e., many loci with variable effect sizes, dominance coefficients, and non-additive interactions) than the simple single-locus model considered here. Although there has been some work on how divergent selection on multiple, possibly interacting, loci impacts genomic differentiation (e.g., (Yeaman et al. 2016; Aeschbacher et al. 2017)), this has not been investigated in the context of hemizygosity (but see (Fusco and Uyenoyama 2011; Fraïsse and Sachdeva 2021)). Second, the model we considered was also relatively simple, ignoring sex-specific effects such as sex-biased migration, sex-specific selection, and the absence of dosage compensation. For instance, Lasne et al. (2017) predicted that sex-specific migration has a large impact on faster X-differentiation in models with strong migration ($m >> s$). Third, our model assumes mammal-like recombination (Betancourt et al. 2004) in which males recombine in autosomes but not in X-chromosomes. This differs from models with sex-specific recombination, in which the sex with hemizygous

chromosomes do not recombine even at diploid autosomes, as seen in *Drosophila* and Lepidoptera (Charlesworth et al. 2018). Fourth, we have considered a parallel dominance fitness landscape and the magnitude of faster-X differentiation might differ for other models (but see Lasne et al. (2017). Finally, we have ignored the effects that removing deleterious mutations with similar effects across populations may have on faster-X differentiation patterns (Charlesworth et al. 1993; Charlesworth et al. 1997). Making precise predictions about chromosome-wide levels in population genomic datasets will require modeling these more complex scenarios, as well as taking into account variation in recombination rate.

Empirical data: Meta-analysis of sex chromosomes vs. autosomes

Our simulations revealed that differences in effective size between hemizygous chromosomes and diploid chromosomes will ensure that the former exhibits higher differentiation under almost any circumstances. Our simulations also predict that, once drift is accounted for, faster-X adaptive differentiation will be most pronounced when gene flow is high. To evaluate these predictions, we searched the literature for genome-wide datasets for which we could obtain differentiation estimates from both autosomes and sex chromosomes. When available, we also recorded whether or not the population/species pairs under consideration were likely to have experienced gene flow during divergence. In total, we obtained 28 datasets that met our criteria for inclusion, of which 24 were from taxa with ZZ/ZW sex determination (Supplementary Table S6). From these datasets we calculated Weir and Cockerham (1984)'s F_{ST} using SNPs from the original studies.

Consistent with other published comparisons of differentiation at sex chromosomes and autosomes (Irwin 2018; Presgraves 2018), we found that 24 out of the 28 cases had higher differentiation at sex chromosomes (Figure 7A). Going a step further, we asked whether faster-X differentiation persisted even after accounting for likely differences in effective population size. We devised a single-sample test in which we resampled the autosomes to create sex-chromosomes with the same number of SNPs as the actual sex chromosomes and adjusted the autosomal F_{ST} by 4/3. After accounting for differences in effective size, 22 out of 28 cases had significantly higher differentiation at sex chromosomes ($p < 0.05$, Supplementary Table S6). We note, however, that our correction for differences in effective size assumes a 50:50 sex ratio. If

taxa have biased sex ratios, this can lead to both false negatives (sex ratios biased towards the homogametic sex) and false positives (sex ratios biased towards the heterogametic sex). Nevertheless, our simulations suggest that overall, this correction is likely to be conservative (Supplementary Figure S11).

We next asked whether taxon pairs that exchanged genes were more likely to exhibit more pronounced faster-X differentiation than those pairs that have diverged in the absence of gene flow. We first looked across all study systems and found no difference between systems with and without gene flow in the proportion of studies that exhibited faster-X differentiation after correcting for effective population size (11/12 for no gene flow; 11/14 for gene flow, Supplementary Table S6). One caveat is that these studies represent diverse study systems, with different amounts of gene flow, different sex chromosomes, and diverse sequencing approaches, which may obscure patterns. To minimize some of these confounding variables, we therefore examined differences among different *Heliconius* population pairs from (Martin et al. 2013). Although all pairs of taxa exhibited evidence of faster-X adaptive differentiation in this dataset (Figure 7B), those pairs experiencing gene flow had significantly higher F_{ST} Z to F_{ST} A ratios (one-tailed p=0.024). Although this trend was noted in the original study (Martin et al. 2013), they attributed it to genetic incompatibilities on the Z chromosome that cause hybrid female sterility. However, our simulations demonstrate that even in the absence of intrinsic genetic incompatibilities, divergent natural selection (e.g., matching locally abundant color morphs) can give rise to a relationship between gene flow and elevated faster-X differentiation.

Our finding that many non-hybridizing taxon pairs exhibit faster-X differentiation after accounting for genetic drift was not predicted by our simulations (see m=0 regions of parameter space for Figure 5 and Supplementary Figures S11 and S12). This could be due to imperfect knowledge of sex ratios, times of split, effective sizes, or gene flow. As discussed above in the summary of simulation results, it is possible that for pairs of populations that diverged more recently, the impact of selection against drift can lead to faster-X differentiation at shorter divergence times. A more systematic analysis of faster-X differentiation with quantitative estimates of gene flow would be a valuable contribution to the literature. Additionally, there may be differences between sex chromosomes and autosomes besides ploidy that can lead to elevated differentiation on sex chromosomes. For example, higher gene density, increased mutation rate,

and increased prevalence of sex-biased genes may all give rise to faster-X differentiation (Meisel and Connallon 2013).

Empirical data: faster-X differentiation in a haplodiploid species pair

Because they lack true sex chromosomes, haplodiploid taxa are potentially powerful models for investigating the impact of hemizygous selection on population differentiation and species divergence without additional confounding factors. However, faster-X differentiation is difficult to quantify in haplodiploids because they lack chromosomes that are analogous to diploid autosomes and experience the same demographic history. To overcome this limitation, we compared observed haplodiploid differentiation levels to expected differentiation levels obtained via simulating diploid and haplodiploid chromosomes evolving under divergent selection with gene flow under a demographic model inferred from observed data. We applied this strategy to populations of *Neodiprion pinetum* and *N. lecontei*, a pair of hybridizing haplodiploid sister species that differ in host use (Linnen and Farrell 2007; Linnen and Farrell 2008).

Overview of haplodiploid study system

We chose *N. pinetum* and *N. lecontei* not only because they are haplodiploid, but also because we have a good understanding of their basic ecology and life history (Coppel and Benjamin 1965). Both species are highly specialized pine feeders, but while *N. pinetum* feeds only on white pine, *N. lecontei* tends to avoid this host. Differences between their pine host likely generate divergent selection on many different traits (Coppel and Benjamin 1965; Codella and Raffa 2002; Lindstedt et al. 2011; Bendall et al. 2017). For example, differences in pine needle chemistry and thickness are associated with among-species differences in host preference, egg size, female ovipositor morphology, and female egg-laying behaviors. These traits, which together determine the reproductive success of adult females, act as an ecological barrier to gene exchange in sympatric populations (Bendall et al. 2017). This previous work suggests that many regions of the genome are likely to be under divergent selection between these species. Additionally, several observations suggest that *N. pinetum* and *N. lecontei* are connected by gene flow. Both species are widely distributed in eastern North America and have largely overlapping

ranges (Benjamin 1955; Rauf and Benjamin 1980; Linnen and Farrell 2010). Lab crosses between the species produce viable and fertile hybrids that are capable of backcrossing in either direction (Bendall et al. 2017). We have collected putative hybrids in the field that we verified by genetic analysis here (Figure 8), and we have detected evidence of mitochondrial introgression (Linnen and Farrell 2007). Together, the combination of multifarious divergent selection and divergence with gene flow make this an ideal system for understanding the genomic consequences of hemizygosity in haplodiploids.

Demographic analysis

To parameterize our faster-X differentiation simulations, we used ddRAD sequencing to generate genome-wide polymorphism data for sympatric populations of *N. pinetum* (n=23) and *N. lecontei* (n=44) from Lexington, KY (Supplementary Table S7). We used putatively neutral SNPs from intergenic regions to generate a joint population site frequency spectrum (SFS), which we polarized using data from an outgroup species, *N. virginiana*. Using fastsimcoal2 (Excoffier et al. 2013) for model selection and demographic parameter estimation from the unfolded SFS, we found that *N. pinetum* and *N. lecontei* diverged ~1.5×10^6 generations ago, and likely experienced continuous asymmetric migration since then, with *N. lecontei* to *N. pinetum* having the higher migration rate (Figure 8B, Supplementary Table S8). Assuming 1-3 generations per year (Benjamin 1955; Rauf and Benjamin 1980), *N. pinetum* and *N. lecontei* likely diverged between 0.5 and 1.5 miliion years ago. This model provides a good fit to the observed SFS and other summary statistics (Supplementary Figure S13).

Next, we examined genomic patterns of differentiation between *N. lecontei* and *N. pinetum*. There is a large amount of heterogeneity in divergence across the genome, which results in a bimodal density distribution of the per site F_{ST} (Figure Figure 8C). Consistent with a history of selection on genic regions, mean F_{ST} at genic regions was higher than at intergenic regions, irrespective of the estimator and dataset used. For down-sampled 2D-SFS, the weighted Hudson et al. (1992) estimator (F_{ST}H92) was 0.68 *vs.* 0.64 for genic and intergenic SNPs, respectively (mean per site F_{ST}H92=0.43 *vs*. 0.39). For the full dataset, the weighted Weir and Cockerham (1984) F_{ST}WC84=0.65 *vs.* 0.61, and mean per site F_{ST}WC84=0.38 *vs.* 0.35 A permutation test on per site F_{ST} revealed that differences between genic and intergenic regions were significant ($p<0.0001$).

Simulating faster-X differentiation

To determine the influence of hemizygosity on differentiation between *N. lecontei* and *N. pinetum*, we simulated diploid and hemizygous genomes evolving under divergent selection with gene flow according to the fitness model in Figure 1A and estimated demographic history for *N. lecontei* and *N. pinetum* (Figure 8B, Supplementary Table S8). We then compared our observed F_{ST} to simulated expectations to ask: (1) are we in a region of parameter space for which we would expect faster-X adaptive differentiation? and (2) what combinations of selection coefficients and dominance could explain our data?

A comparison between our observed summary statistics (SFS, F_{ST}, number of pairwise differences, d_{xy}, and r^2) for the putatively neutral intergenic regions and summary statistics obtained from neutral simulations ($2Ns = 0$) shows that the demographic model implemented in SLiM is working as expected, and that our simulated diploid and haplodiploid chromosomes do not differ under neutrality (Supplementary Figure S13). We next looked at the mean F_{ST} across all 1000 simulations for each starting allele frequency, dominance, and selection coefficient combination. These combined simulations can be thought of as a divergence history in which, on average, there is a divergently selected site every 500 kb. Regardless of the combination of dominance and minor allele frequency, we found that our observed F_{ST} for genic regions always corresponded to regions of parameter space where $s>0$ and where faster-X differentiation would be expected (i.e., the location where observed genic F_{ST} intersects expected F_{ST} for the hemizygous case always exceeds the expected F_{ST} for the diploid case; Figure 9). Under our estimated divergence model, faster-X adaptive differentiation was most pronounced when the divergently selected allele was recessive.

The selection coefficient needed to explain our observed genic F_{ST} was strongly influenced by both dominance and starting minor allele frequency (Figure 9). For example, assuming that selected alleles are recessive and have a starting allele frequency of 0.01, a selection coefficient of s=0.30 on a hemizygous allele would be required to generate the level of differentiation observed for our genic dataset (Figure 9B), a perhaps unrealistically high selection coefficient. By contrast, for more common alleles (q=0.10), a selection coefficient of s~0.05 is sufficient to explain genic F_{ST}, regardless of dominance (Figure 9B,D). These differences likely reflect the changing importance of differential allele loss in generating faster-X

differentiation. At lower allele frequencies, many alleles are lost to drift, requiring stronger selection to reach the same average differentiation levels. At higher starting allele frequencies, the increased efficacy of selection against migrants becomes more important to generating faster-X adaptive differentiation.

Of course, the genetic architecture of host adaptation is likely to be much more complex than modeled in our simulations. We know that many traits, and therefore many loci, are involved in host adaptation in this and many other plant-feeding insect systems (Nosil and Sandoval 2008; Mcbride and Singer 2010; Gompert et al. 2013; Bendall et al. 2017). And these loci are likely to vary in starting allele frequencies, dominance coefficients, fitness models, and selection coefficients. We also have not accounted for background selection in our simulations. Additional empirical data and simulation work will be needed to explore these more complex scenarios. Nevertheless, our simulations do encompass four very different dominance and standing genetic variation scenarios, suggesting that hemizygosity has likely increased adaptive differentiation in these hybridizing haplodiploids.

Conclusions

Classic faster-X theory demonstrates how increased retention of recessive alleles can give rise to increased rates of adaptive substitutions in hemizygous chromosomes. Here we show that when populations diverge with gene flow, this mechanism works in concert with a second mechanism – increased efficacy of selection against immigrant alleles – to elevate adaptive differentiation on sex chromosomes and haplodiploid genomes relative to their diploid counterparts. This additional mechanism explains why faster-X adaptive differentiation, unlike faster-X substitution, occurs even when selected alleles are codominant. We also show that faster-X adaptive differentiation mechanisms can impact even fairly weakly linked neutral variation, resulting in less opportunity for recombination in hemizygous chromosomes. This can increase the chances of establishment of other mutations under divergent selection, ultimately reducing the genome-wide gene flow experienced by diverging populations. Furthermore, our simulations show that faster-X differentiation gives rise to heterogeneous diversity and differentiation patterns with detectable signatures in genome-wide datasets. Finally, our empirical data suggest that conditions that give rise to faster-X adaptive differentiation are widespread in nature, possibly indicating that many pairs of taxa likely diverged with gene flow

and that divergent selection can have a substantial impact on both selected and neutral variation in hemizygous chromosomes.

Methods

Model

We considered an isolation with migration model with two populations with effective size N_e that diverged T_{div} generations ago from an ancestral population with the same size (N_e), and since then exchange migrants at a constant and symmetric migration rate $m=m_{12}=m_{21}$. At the selected locus we considered a "parallel dominance" fitness model in which the derived allele *a* is favored in population 1 and allele *A* (ancestral allele) is favored in population 2, its dominance is the same irrespective of the population, and with dosage compensation in the heterogametic sex for hemizygous loci, parameterized as shown in Figure 1 (as in Moran (1959); Lasne et al. (2017). Our model assumes there are separate sexes, with equal numbers of males and females, without sex-specific migration or selection, and similar distribution of offspring numbers in males and females.

Deterministic simulations

We investigated the migration-selection dynamics in diploid and hemizygous loci with deterministic simulations that included separate sexes, following the allele trajectories of two alleles *a* and *A* at a single locus under divergent selection at discrete generations. We assumed there is no mutation, recombination, or drift and that selection and migration are both symmetrical. We consider generation 0 to be the onset of selection (colonization of new habitat with open niches) and used an R script to simulate allele trajectories for T_{div}=100,000 generations from an initial frequency of q_0 of allele *a* in both populations. At each generation we measured differentiation with F_{ST} based on the allele frequencies in the two populations (using eq. 11 in Lasne et al. 2017). We simulated hemizygous loci and diploid loci under two dominance coefficients ("recessive": h = 0.01; "codominant": h = 0.5; with *A* dominant to *a*), five starting allele frequencies (q_0 = 0.00001, 0.0001, 0.01, 0.10, 0.50), and a wide range of migration rates and selection coefficients (Supplementary Table 1).

Time to equilibrium: The time to equilibrium was defined as the time point when allele frequencies remained similar across generations. To avoid numerical issues, this was defined as

the time when two conditions were met: the allele frequency changed by less than $\varepsilon * p(T)$ over w generations ($p(t+w)-p(t) < \varepsilon * p(T)$), and it also changed less than $\varepsilon * p(T)$ in the last generation T ($p(T)-p(T-1) < \varepsilon * p(T)$), where $p(t)$ is the allele frequency at time t, T is the number of generations in the simulations ($T=10^5$), w is the generation difference (w=1000), and ε is an error term ($\varepsilon=10^{-12}$).

Migration threshold: Assuming that a new mutation appears in the population where it is beneficial, the migration threshold is defined as the migration rate below which populations can diverge at that locus (Yeaman and Otto 2011). We estimated the migration threshold for diploid and hemizygous loci based on deterministic simulations with an initial frequency of $q_0=10^{-5}$ (mimicking a new mutation). For a given selection coefficient, we considered that this threshold corresponds to the migration rate at which populations become differentiated, i.e., F_{ST} becomes larger than zero. To avoid precision issues we considered that was the case when $F_{ST}>10^{-10}$ after 100,000 generations. To estimate the migration threshold from F_{ST} values obtained at a grid of points in the parameter space of selection coefficients and migration rates, we performed a 2D-barycentric interpolation. For comparison with analytical results, we also computed the expected threshold for diploid chromosomes, using Yeaman and Otto's (2011) approximation to the migration threshold under a continent-island model.

Stochastic simulations

We used SLiM v3 (Haller and Messer 2019) to simulate 500-kb chromosomes evolving via divergent selection, gene flow and genetic drift. To compare diploid with hemizygous chromosomes under the same conditions, we performed independent simulations for autosomes (diploid) and X-chromosomes (hemizygous) according to an isolation with migration model (Figure 1B). First, to enable the ancestral population to reach mutation-drift equilibrium, we simulated neutral evolution of an ancestral population with an effective size of $2N_e$, a mutation rate of $\mu=2.5\text{x}10^{-7}$/bp/generation and a recombination rate of $r=\mu=2.5\text{x}10^{-7}$/bp/generation for 10,000 generations (>$4N_e$ generations). Second, to simulate divergence with gene flow, we considered that the ancestral population splits into two equally sized populations ($2N_e$) that exchange migrants at a constant and symmetrical migration rate $m=m_{12}=m_{21}$ for T_{div}=2000 generations. We chose a split time of 2000 generations because this corresponds to moderate divergence with a scaled time $T_{div}/(4N_e)$=2/3. This is within the range of values estimated for

pairs of closely related populations and species across many taxa (Pinho and Hey 2010; Hey and Pinho 2012), but lower than the threshold of $T_{div}/(4N_e)>1$ (and $2N_em<1$) proposed by Hey and Pinho (2012) as a diagnostic for fully independent species.

Divergent selection occurs at a locus located in the middle of the 500-kb region. As in the deterministic simulations, we used a "parallel dominance" fitness model (Figure 1A). We simulated diverging populations under all possible combinations of seven selection coefficients (scaled $2N_es$ ~ 0, 10, 20, 40, 80, 100, 200), four migration rates (scaled $2N_em$ ~ 0.0, 0.5, 2.5, 5.0), two dominance coefficients (recessive h=0.01 and codominant h=0.50), and four different starting allele frequencies ($q_0 = 1/(2N_e)$, 0.01, 0.10, and 0.50; Supplementary Table S1). The selection and migration rates were chosen based on regions of parameter space that reached equilibrium and exhibited faster-X differentiation in our deterministic simulations ($s>m$), plus the neutral case (s=0) and the no-migration case (m=0). To investigate the impact of recombination rate on linked variation we repeated a subset of these conditions (with q_0=0.10 and 0.50) under a lower recombination rate ($r=0.1\mu= 2.5\text{x}10^{-8}$/bp/generation).

Scaled vs unscaled simulations: To tease apart the effects of hemizygosity (increased selection efficacy) and effective size (increased drift), we performed two types of simulations, each investigating all parameter combinations described above: "scaled", in which model parameters were modified such that the hemizygous and diploid chromosomes experience equivalent effective levels of drift, migration, and recombination; and "unscaled", corresponding to the comparison of autosomes with X or Z chromosome (Supplementary Table S1). In a population with N_F females and N_M males, the effective size of autosomes is $N_A=(4N_MN_F)/(N_M+N_F))$ and of X (or Z) chromosome is $N_X=(9N_MN_F)/(4N_M+2N_F)$ (Wright 1969, Mendez 2017). Thus, the ratio $x=N_X/N_A$ of X to autosome effective sizes depends on the number of individuals from each sex. Defining the sex-ratio as the proportion of males $sr=N_M/(N_M+N_F)$, $x=N_X/N_A$ simplifies to $x=(9/8)(1/(1+sr))$, recovering x=3/4 for a sex-ratio of 50:50 (sr=0.50). For the scaled simulations, we adjusted the N_e to ensure that both the diploid and hemizgyous chromosomes have $2N_e$=1500. This is the effective size of a hemizygous locus with N=1000 individuals (500 females with two copies and 500 males with one copy). This corresponds in the diploid case to $N_D=x\,N$ individuals, where x=3/4 for a 0.50 sex-ratio, resulting in N_D=750 individuals (N_F=375 females and N_M=375 males). To ensure that the average recombination rate

was the same for diploid and hemizygous chromosomes, we multiplied the diploid recombination rate by 2/3 since the hemizygous chromosome spends 2/3 of its time in the sex in which it recombines, assuming that diploid chromosomes recombine in both sexes (Betancourt et al. 2004; Lohmueller et al. 2010). This scaling is important because average recombination rate can impact linked variation and there is evidence that sex chromosomes and haplodiploid genomes have average recombination rates comparable to autosomes, despite the presence of non-recombining individuals (Kong et al. 2002; Wilfert et al. 2007). To confirm that the scaling was done correctly, we verified that the values of several summary statistics measuring diversity, differentiation and LD were identical for simulations for hemizygous and diploid chromosomes, and that they converged to the expected values under neutrality (Supplementary Figure S14). For the unscaled, simulations were done with N_F=375 females and N_M=375 males, corresponding to an effective size of $2N_A$=1500 for autosomes (the same as in the scaled simulations) and $2N_X$=1125 for the X-chromosome (Supplementary Table S1).

Summary statistics: We simulated 1000 replicates for each different parameter combination for both hemizygous chromosomes and diploid chromosomes, for scaled and unscaled cases (Supplemental Table S1). For each replicate, we followed the trajectories of allele frequencies at the selected site in both populations, which were used to compute (i) the number of simulations where the derived allele *a* was retained in population 1; (ii) the time to reach an average allele frequency differentiation between population 1 and 2 larger than found at selection-migration equilibrium in deterministic simulations, which is analogous to the time to fixation of differential alleles in two populations; and (iii) F_{ST} based on the mean population allele frequencies at the last generation (using eq. 11 in Lasne et al. 2017). To investigate patterns of linked variation in samples rather than at the population level, in the last generation we sampled 20 chromosomes of 500Kb from each population. For each parameter combination, we computed average nucleotide diversity, D_{xy} and weighted F_{ST} across simulations using Hudson estimator (Bhatia et al. 2013), averaged across all SNPs of the 500Kb chromosome, and at continguous non-overlapping 20Kb windows. To measure patterns of linkage disequilibrium, we computed the average r^2 between all pairs of SNPs within 20Kb windows. To account for the effect of loss of the derived allele *a*, we used two approaches: in the "all simulations" approach, the mean of summary statistics (e.g., F_{ST}) is computed across all simulations, whereas in the "conditional" approach, the mean of summary statistics is computed only across simulations

where the derived allele was retained (Figure 1C). Cases with less than 10 simulations retained were treated as missing data.

Adjusting F_{ST} for comparing autosomes and sex-chromosomes: For the unscaled simulations, the F_{ST} is expected to be higher in the X (or Z) chromosome even under neutrality due to their lower effective size. To account for this effect we considered two approaches to adjust the F_{ST} values that could be potentially applied to empirical data: (i) multiply the autosome estimated $F_{ST}(A)$ by the factor $f_{AX}=(1/x)$ to obtain an adjusted $F_{ST}(A_{adj})=f_{AX}\,F_{ST}(A)$, where x is the ratio of X-chromosome to autosome effective sizes (see above), comparing the adjusted $F_{ST}(A_{adj})$ with the X-chromosome $F_{ST}(X)$; and (ii) divide F_{ST} values by the corresponding neutral values, comparing $F_{ST}(X)/(\text{neutral } F_{ST}(X))$ to $F_{ST}(A)/(\text{neutral } F_{ST}(A))$. The first approach does not require data from neutral regions as it is based on deriving the expected F_{ST} as a function of the relative effective sizes. This was obtained by expressing F_{ST} in terms of expected coalescent times for a sample of 2 lineages within (t_w) or between (t_b) populations, $F_{ST}=(t_b-t_w)/t_b$ (Slatkin 1991). For an isolation model of two populations with equal N that split T_{div} generations ago $t_w=2N$, $t_b=T_{div}+2N$ and $F_{ST}=T_{div}/(T_{div}+2N)$. Noting that the ratio of X and autosome effective sizes $x=N_X/N_A=(9/8)(1/(1+sr))$ depends on the sex-ratio sr (see above), we obtain the expected ratio of F_{ST} as $E[F_{ST}(X)/F_{ST}(A)]=(T_{div}+2N_A)/(T_{div}+x2N_A)$. This depends on the time of divergence, which is usually unknown. Here we take a conservative approach by considering its maximum value, which is $(1/x)$ in the limit as T_{div} approaches zero. The same rationale can be applied to a two island model with symmetrical migration m, where $t_w=2N$, $t_b=2N+(1/(2m))$ and $F_{ST}=1/(4Nm+1)$, to derive that $E[F_{ST}(X)/F_{ST}(A)]=(1+4Nm)/(1+x4Nm)$. With migration, the maximum expected F_{ST} ratio is again $(1/x)$ when $4Nm$ tends to infinity. For both isolation and migration cases considered, with a sex-ratio of 0.50 this results in $E[F_{ST}(X)/F_{ST}(A)]=4/3$, recovering results for an isolation model using a different approach (Keinan et al. 2009). For the simulations we used this conservative adjustment factor $f_{AX}=(4/3)$ as it was also used in the meta-analysis (see below), but note that it could be adjusted to reflect system specific sex-ratios, migration rates and divergence times. The second approach can be applied in empirical datasets by using F_{ST} at putative neutral regions (e.g., intergenic) in both autosomes and X (or Z) chromosomes as a reference.

Comparing hemizygous and diploid chromosomes

To measure faster-X differentiation we compared several statistics (e.g., F_{ST} and time to equilibrium) obtained for hemizygous (H) and diploid (D) loci by considering their ratio (H/D), e.g. F_{ST} (H/D). For F_{ST}, to avoid divisions by zero and numerical issues due to ratios of small values, we set all F_{ST} less than a threshold ε to that threshold. For the deterministic simulations we considered $\varepsilon=10^{-4}$, for stochastic simulations at selected locus $\varepsilon=0.02$ and for linked sites $\varepsilon=10^{-3}$. To account for sampling noise in stochastic simulations, all ratios between 0.95 and 1.05 were set to 1.00, i.e., only effects larger than 5% effect were considered as differences between hemizygous and diploid loci. To visualize how different combinations of selection coefficients and migration rates impacted the magnitude of faster-X differentiation, we used a 2D-barycentric interpolation of the ratios of statistics across the selection-migration parameter space using R (R Core Team 2020) with packages geometry (Habel et al. 2019) and ggplot2 (Wickham 2016) to produce heat maps. The interpolation was performed with selection coefficients and migration rates on a log10 scale, and hence to include the neutral (s=0) and no migration (m=0) cases we replaced those undefined log(0) values by an arbitrary small value.

Meta-analysis

We performed a meta-analysis comparing mean F_{ST} between autosomes and X/Z chromosomes. We collected data from 11 published studies for a total of 28 taxon pairs (Supplementary Table S6). For a dataset to be included, we required access a VCF file for genome scale data (e.g. RAD, GBS, whole genome resequencing). There had to be no known inversions in the sex chromosomes, and the sex chromosomes had to be heteromorphic. We excluded any study that had pooled sequencing.

We used SNPs that had been previously called in the original studies. If the original study accounted for difference in sex chromosome ploidy between males and females for computing F_{ST} at sex chromosomes, we retained their methodology. Otherwise we only kept the homogametic sex. We accomplished this by removing low heterozygosity individuals (<1% at sex chromosome) if sex was not stated. We calculated F_{ST} according to Weir and Cockerham (1984) using a combination of VCFtools, diveRsity, and custom R scripts (Weir and Cockerham 1984; Danecek et al. 2011; Keenan et al. 2013). We calculated the mean per site F_{ST} separately

for autosomes and sex chromosomes. To test if sex chromosomes differed from autosomes in mean F_{ST} we used a non-parametric permutation approach, permuting loci between autosomes and sex-chromosomes. To account for the difference in N_e we adjusted the resampled average F_{ST} values of autosomes by f_{AX}=4/3 (see details above). We performed 1,000,000 permutations to compute the sampling distribution of difference between means under the null hypothesis (H_0: $F_{ST}(X)=F_{ST}(A_{Adj})$). To compute the p-value we compared our observed difference in mean F_{ST} to the sampling distribution. To determine whether observed ratios of sex-chromosome F_{ST} to autosome F_{ST} differed between *Heliconius* taxon pairs that diverged with or without gene flow, we used the "wilcox.test" function in R to implement a Wilcoxon rank sum exact test. Because our simulation results predicted higher ratios in the presence of gene flow, we reported one-tailed p-values.

Analysis of genomic data from Neodiprion *sawflies*

Population sampling

N. pinetum and *N. lecontei* have largely overlapping ranges in the eastern part of the United States and all sampling occurred in the overlapping region. We sampled 23 individuals from one population of *N. pinetum* in Kentucky. There are three population clusters of *N. lecontei;* North, Central, and South (Bagley et al. 2017). We sampled 44 *N. lecontei* individuals from Kentucky. This population is sympatric with the sampled *N. pinetum* and is part of the Central *N. lecontei* cluster. Additionally, we sampled 3 morphological female hybrids based on intermediate coloration from Kentucky and 1 lab reared female F_1 as a control (Supplementary Table S7).

DNA sequencing

We extracted DNA using a CTAB/phenol-chloroform-isoamyl alcohol method (Chen et al. 2010). We visualized the DNA on a 0.8% agarose gel to confirm quality. To quantify the DNA we used a Quant-iT High-Sensitivity DNA Assay Kit (Invitrogen – Molecular Probes, Eugene, OR, USA). For *N. pinetum*, *N. lecontei*, and hybrids we used a modified protocol ddRAD sequencing protocol from Bagley et al. (2017) and Peterson et al. (2012). We fragmented the DNA using NlaIII and EcoRI. We assigned each individual along with additional samples from other projects to one of eight libraries. During adapter ligation, we assigned each

sample one 48 unique in-line barcodes (Supplementary Table S7). We used the 5-10 bp variable length barcodes used in Burford Reiskind et al. (2016). We then pooled each group of samples and size selected for 379-bp fragment (+/- 76bp) on a PippinPrep (Sage Science, Beverly, MA). We did 12 rounds of high-fidelity PCR amplification (Phusion High-Fidelity DNA Polymerase, NEB, Ipswich, MA) using PCR primers that included one of 12 unique Illumina multiplex read indices (Supplementary Table S7). To allow for the detection of PCR duplicates, we included a string of 4 degenerate bases next to the Illumina read index (Schweyen et al. 2014). We used a Bioanalyzer 2100 (Agilent, Santa Clara, CA) to check library quality. The libraries were sequenced at the University of Illinois' Roy J. Carver Biotechnology Center, using two lanes of Illumina HiSeq 4000 150 bp single-end reads.

DNA processing and variant calling

We aligned the demultiplexed reads to the *N. lecontei* reference genome (Nlec1.1 GenBank assembly accession number- GCA_001263575.2) using the very sensitive setting in bowtie2 (Langmead and Salzberg 2012; Vertacnik and Linnen 2015; Linnen et al. 2018). We only retained reads that aligned to one locus in the reference genome and had a phred score greater than 30. We removed PCR duplicates using a custom script. We called SNPs in samtools (Li et al. 2009). Male and female larvae are morphologically indistinguishable. To confirm that all of the individuals were female, we examined heterozygosity and excluded individuals with unusually low heterozygosity as putative haploid males (as in Bagley et al. 2017). No individuals were excluded. We required all sites to have a minimum of 7x coverage and 50% missing data or less. We also removed SNPs with significantly more heterozygotes than expected under Hardy-Weinberg equilibrium when pooling all individuals (an indicator of genotyping/mapping error) and a minor allele frequency (MAF) < 0.01. We removed any individual that was missing more than 70% of the data. We performed all filtering in VCFtools (Danecek et al. 2011). After filtering we had 35,649 SNPs when including the hybrids and 36,935 SNPs without the hybrids.

Population structure, demographic analysis, and divergence summary statistics

To confirm that our morphological hybrids were genetically admixed we performed Admixture with K =1- 5 for Kentucky *N. lecontei* and *N. pinetum*, and hybrids (wild caught and lab reared). We ran 100 replicates per K and chose the K with the lowest CV score (Supplementary Table S9). To further test for gene flow we performed demographic modeling

based on the site frequency spectrum (SFS) using the composite likelihood method implemented in fastsimcoal2 (Excoffier et al. 2013). To minimize the impact of selection on demographic history estimates, we used SNPs that were 1 kb away from the start or end of a gene so that we only used putatively neutral sites based on NCBI *Neodiprion lecontei* Annotation Release 100, updated to GCA_001263575.2 . We used the same filtering as above except without the MAF filter applied. Furthermore, to avoid biases in the SFS we only considered genotypes with a depth of coverage larger than 10x and within the range of (1/3) to twice the median depth of coverage per individual. To build the 2D-SFS without missing data, each scaffold was divided into non-overlapping 50Kb blocks (keeping only blocks where the median distance between SNPs was larger than 2bp), and SNPs without missing data were obtained for each block by downsampling four and six females from *N. pinetum* and *N. lecontei*, respectively. This resulted in a downsampled dataset with 9,994 SNPs. To polarize the ancestral/derived state of alleles and obtain the unfolded 2D-SFS we used sequence data from an outgroup species, *Neodiprion virginiana,* based on whole genome sequencing of a single *N. virginianus* female (Vertacnik 2020). For *N. virginiana* we used 150 PE on a Nextseq at Georgia Genomics Facility. Library preparation and sequencing were both completed at the sequencing facility. We removed the adapters using cutadapt 1.16 and contaminants using the standard and pine databases in Kraken (Martin 2011; Wood and Salzberg 2014). We followed the filtering strategy for *N. lecontei* and *N. pinetum*, except for filtering on PCR duplicates as the library preparation differed from the other samples.

We tested five alternative demographic models: 1) divergence without gene flow, 2) divergence with continuous bidirectional migration, 3) divergence in isolation followed by a single bout of secondary contact (unidirectional gene flow), 4) divergence with bidirectional migration that stops before divergence is complete, and 5) divergence in isolation followed by continuous secondary contact (bidirectional). All models except the model of continuous gene flow had an equal number of parameters, so we compared their likelihoods directly (Supplementary Table S8). We ran each model 100 times starting from different parameter combinations, each run with 50 optimization cycles (-l50) and approximating the expected SFS with 100,000 coalescent simulations (-n100000). We selected the run with the highest likelihood in order to estimate parameter values. We computed F_{ST} for *N. lecontei* and *N. pinetum* in VCFtools per site on the non-down sampled data set to look at genome-wide patterns of

divergence (Danecek et al. 2011). We also computed the weighted F_{ST} (Hudson estimator) based on the downsampled 2D-SFS for both the intergenic (> 1 Kb from gene with 9,994 SNPs) and genic (<1 Kb from a gene with 11,073 SNPs) regions to compare with simulations (see below). We focus on the downsampled 2D-SFS data for comparisons with simulations, as they were used to infer the demographic history model implemented in simulations.

Simulating faster-X differentiation for haplodiploid Neodiprion *sawflies*

To determine the influence of haplodiploidy (hemizygosity) on adaptive differentiation of *N. lecontei* and *N. pinetum*, we used SLiM v3 to simulate 500-kb chromosomes with a site under divergent selection (position 250Kb) according to the inferred demographic history. Because white pine is the derived host plant, we modeled *N. pinetum* as population 1 where derived allele *a* is favoured, and *N. lecontei* as population 2. For these simulations, we also assumed a sex ratio of 30 males:70 females (Harper et al. 2016). We compared haplodiploids with equivalent diploid populations with the same levels of drift, migration, mutation rates and recombination, as done for the "scaled" simulations (see above). To reduce the computational burden of forward SLiM simulations we re-scaled parameters such that under neutrality, the SFS obtained with SLiM was identical to the expected SFS obtained under the demographic history inferred with fastsimcoal2. This was achieved by ensuring that the scaled mutation rate $4N_A\mu L$ at a locus with L sites was identical in both cases, where N_A is the ancestral effective size and μ is the mutation rate per site per generation. By considering a mutation rate two order of magnitude higher (μ=3.50x10^{-7} rather than the 3.50x10^{-9} /bp/generation used for SFS-based inference) and that L=500Kb chromosomes in SLiM corresponds to L=50Kb in fastsimcoal2, the haploid effective population sizes were three orders of magnitude lower (328 for *N. pinetum*, 1093 for *N. lecontei* and 1982 for the ancestral population) and migration rates three orders of magnitude higher (3.64x10^{-4} into *N. pinetum*, 1.71x10^{-5} into *N. lecontei*). The times of split were scaled accordingly, resulting in 1548 generations (rather than 1.54x10^{6}). To obtain the number of individuals N in SLiM that correspond to the above haploid effective sizes accounting for a sex-ratio $sr=N_M/(N_F+N_M)=0.30$ we used the expressions $N_e=(4N_MN_F)/(N_M+N_F))$ for diploids and $N_e=(9N_MN_F)/(4N_M+2N_F)$ for haplodiploids (Wright 1969; Mendez 2017), where N_F is the number of females and N_M is the number of males. Noting that $N=N_F+N_M$ and replacing $N_M=srN$ and $N_F=(1-sr)N$ these expressions simplify to $N_e=4Nsr(1-sr)$ and $N_e=(9Nsr(1-sr))/(2(1+sr))$. Solving for the number of

individuals we obtain $N=N_e/(4sr(1-sr))$ for diploids and $N=(2(1+sr)N_e)/(9sr(1-sr))$ for haplodiploids. We assumed that recombination rate was on the same order as mutation rate, i.e. $r=\mu$, adjusting the recombination rate for diploids by (2/3) as done for the scaled simulations (see above). Because the per-locus selection estimate is unknown, we simulated differentiation and under a wide range of selection coefficients. We also simulated all combinations of two dominance coefficients (h = 0.01 and 0.50) and two starting allele frequencies (q_0 = 0.10 and 0.50).

Data availability

All the scripts used for deterministic simulations (R scripts), SliM v3 simulations (bash and Slim input files) and analysis of results (R scripts) are available on VCS's github page (https://github.com/vsousa/EG_cE3c). All the data will be deposited on SRA and available upon acceptance for publication in a peer reviewed journal.

Acknowledgements

We thank members of the Linnen lab for assistance with collection and rearing of pine sawflies. CRL was funded by the National Science Foundation (DEB-CAREER-1750946 and DEB-1257739). RKB was funded by a USDA-NIFA pre-doctoral fellowship (2015-67011-22803). VCS was funded by Portuguese National Science Foundation ("Fundação para a Ciência e a Tecnologia" - FCT) through individual grants CEECIND/02391/2017 and CEECINST/00032/2018/CP1523/CT0008, by EU H2020 program (Marie Skłodowska-Curie grant 799729) and by the FCT strategic projects UIDB/00329/2020 granted to cE3c. For computing resources, we thank the University of Kentucky Center for Computational Sciences and the Lipscomb High Performance Computing Cluster, as well as the INCD (https://incd.pt/), which is funded by FCT and FEDER (project 01/SAICT/2016 nº 022153).

Conflict of interest

The authors declare no conflict of interest.

References

Aeschbacher S, Selby JP, Willis JH, Coop G. 2017. Population-genomic inference of the strength and timing of selection against gene flow. *Proceedings of the National Academy of Sciences* 114:7061–7066.

Avery PJ. 1984. The population genetics of haplo-diploids and X-linked genes. *Genetical Research* 44:321–341.

Bagley RK, Sousa VC, Niemiller ML, Linnen CR. 2017. History, geography and host use shape genomewide patterns of genetic variation in the redheaded pine sawfly (Neodiprion lecontei). *Molecular Ecology* 26:1022–1044.

Barrett RDH, Schluter D. 2008. Adaptation from standing genetic variation. *Trends in Ecology and Evolution* 23:38–44.

Barton NH, Bengtsson BO. 1986. The barrier to genetic exchange between hybridising populations. *Heredity* 56:357–376.

Bendall EE, Vertacnik KL, Linnen CR. 2017. Oviposition traits generate extrinsic postzygotic isolation between two pine sawfly species. *BMC Evolutionary Biology* 17:1–15.

Benjamin DM. 1955. The Biology and Ecology of the Red-headed Pine Sawfly. U.S. Department of Agriculture

Betancourt AJ, Kim Y, Orr HA. 2004. A pseudohitchhiking model of X vs. autosomal diversity. *Genetics* 168:2261–2269.

Bhatia G, Patterson N, Sankararaman S, Price AL. 2013. Estimating and interpreting FST: the impact of rare variants. *Genome Research* 23:1514–1521.

Burford Reiskind MO, Coyle K, Daniels H V., Labadie P, Reiskind MH, Roberts NB, Roberts RB, Schaff J, Vargo EL. 2016. Development of a universal double-digest RAD sequencing approach for a group of nonmodel, ecologically and economically important insect and fish taxa. *Molecular Ecology Resources* 16:1303–1314.

Campbell P, Good JM, Nachman MW. 2013. Meiotic sex chromosome inactivation is disrupted in sterile hybrid male house mice. *Genetics* 193:819–828.

Charlesworth B. 2012. The Role of Background Selection in Shaping Patterns of Molecular Evolution and Variation: Evidence from Variability on the *Drosophila X* Chromosome. *Genetics* 191:233–246.

Charlesworth B, Campos JL, Jackson BC. 2018. Faster-X evolution: Theory and evidence from *Drosophila*. *Molecular Ecology* 27:3753–3771.

Charlesworth B, Coyne JA, Barton NH. 1987. The Relative Rates of Evolution of Sex Chromosomes and Autosomes. *The American Naturalist* 130:113–146.

Charlesworth B, Morgan MT, Charlesworth D. 1993. The effect of deleterious mutations on neutral molecular variation. *Genetics* 134:1289–1303.

Charlesworth B, Nordborg M, Charlesworth D, others. 1997. The effects of local selection, balanced polymorphism and background selection on equilibrium patterns of genetic diversity in subdivided populations. *Genetical Research* 70:155–174.

Chen H, Rangasamy M, Tan SY, Wang H, Siegfried BD. 2010. Evaluation of Five Methods for Total DNA Extraction from Western Corn Rootworm Beetles. *PLoS ONE* 5:e11963.

Codella SG, Raffa KF. 2002. Desiccation of Pinus foliage induced by conifer sawfly oviposition: effect on egg viability. *Ecological Entomology* 27:618–621.

Connallon T, Singh ND, Clark AG. 2012. Impact of Genetic Architecture on the Relative Rates of X versus Autosomal Adaptive Substitution. *Molecular Biology and Evolution* 29:1933–1942.

Coppel H, Benjamin D. 1965. Bionomics of the Nearctic Pine-Feeding Diprionids. *Annual Review of Entomology* 10:69–96.

Cruickshank TE, Hahn MW. 2014. Reanalysis suggests that genomic islands of speciation are due to reduced diversity, not reduced gene flow. *Molecular Ecology* 23:3133–3157.

Danecek P, Auton A, Abecasis G, Albers CA, Banks E, Depristo MA, Handsaker RE, Lunter G, Marth GT, Sherry ST, et al. 2011. The variant call format and VCFtools. *Bioinformatics* 27:2156–2158.

Excoffier L, Dupanloup I, Huerta-Sánchez E, Sousa VC, Foll M. 2013. Robust demographic inference from genomic and SNP data.Akey JM, editor. *PLoS Genetics* 9:e1003905.

Feder J L, Egan SP, Nosil P. 2012. The genomics of speciation-with-gene-flow. *Trends in Genetics* 28:342–350.

Feder Jeffrey L., Gejji R, Yeaman S, Nosil P. 2012. Establishment of new mutations under divergence and genome hitchhiking. *Philosophical Transactions of the Royal Society B: Biological Sciences* 367:461–474.

Feder JL, Nosil P. 2010. The efficacy of divergence hitchhiking in generating genomic islands during ecological speciation. *Evolution* 64:1729–1747.

Fraïsse C, Sachdeva H. 2021. The rates of introgression and barriers to genetic exchange between hybridizing species: sex chromosomes vs autosomes. *Genetics* 217:iyaa025.

Frank SA. 1991. Divergence of meiotic drive-suppression systems as an explanation for sex-biased hybrid sterility and inviability. *Evolution* 45:262–267.

Fusco D, Uyenoyama MK. 2011. Sex-specific incompatibility generates locus-specific rates of introgression between species. *Genetics* 189:267–288.

Gompert Z, Lucas LK, Nice CC, Fordyce JA, Alex Buerkle C, Forister ML. 2013. Geographically multifarious phenotypic divergence during speciation. *Ecology and Evolution* 3:595–613.

Gronau I, Hubisz MJ, Gulko B, Danko CG, Siepel A. 2011. Bayesian inference of ancient human demography from individual genome sequences. *Nature Genetics* 43:1031–1034.

Habel K, Grasman R, Gramacy RB, Mozharovskyi P, Sterratt DC. 2019. geometry: Mesh Generation and Surface Tessellation. Available from: https://cran.r-project.org/package=geometry

Haller BC, Messer PW. 2019. SLiM 3: Forward Genetic Simulations Beyond the Wright–Fisher Model. *Molecular Biology and Evolution* 36:632–637.

Harper KE, Bagley RK, Thompson KL, Linnen CR. 2016. Complementary sex determination, inbreeding depression and inbreeding avoidance in a gregarious sawfly. *Heredity* 117:326–335.

Hedrick PW, Parker JD. 1997. Evolutionary genetics and genetic variation of haplodiploids and X-linked genes. *Annual Review of Ecology and Systematics* 28:55–83.

Hermisson J, Pennings PS. 2005. Soft Sweeps. *Genetics* 169:2335–2352.

Hey J, Pinho C. 2012. Population genetics and objectivity in species diagnosis. *Evolution* 66:1413–1429.

Hoban S, Bertorelle G, Gaggiotti OE. 2012. Computer simulations: tools for population and evolutionary genetics. *Nature Reviews Genetics* 13:110–122.

Höllinger I, Hermisson J. 2017. Bounds to parapatric speciation: A Dobzhansky-Muller incompatibility model involving autosomes, X chromosomes, and mitochondria. *Evolution* 71:1366–1380.

Hudson RR, Slatkin M, Maddison WP. 1992. Estimation of levels of gene flow from DNA sequence data. *Genetics* 132:583–589.

Hurst LD, Pomiankowski A. 1991. Causes of sex ratio bias may account for unisexual sterility in hybrids: a new explanation of Haldane's rule and related phenomena. *Genetics* 128:841–858.

Irwin DE. 2018. Sex chromosomes and speciation in birds and other ZW systems. *Molecular Ecology* 27:3831–3851.

Karasov T, Messer PW, Petrov DA. 2010. Evidence that Adaptation in Drosophila Is Not Limited by Mutation at Single Sites. *PLoS Genetics* 6:e1000924.

Keenan K, McGinnity P, Cross TF, Crozier WW, Prodöhl PA. 2013. diveRsity : An R package for the estimation and exploration of population genetics parameters and their associated errors.O'Hara RB, editor. *Methods in Ecology and Evolution* 4:782–788.

Keinan A, Mullikin JC, Patterson N, Reich D. 2009. Accelerated genetic drift on chromosome X during the human dispersal out of Africa. *Nature Genetics* 41:66–70.

Kimura M, Ohta T. 1971. On the Rate of Molecular Evolution. *Journal of Molecular Evolution* 1:1–17.

Kong A, Gudbjartsson DF, Sainz J, Jonsdottir GM, Gudjonsson SA, Richardsson B, Sigurdardottir S, Barnard J, Hallbeck B, Masson G, et al. 2002. A high-resolution recombination map of the human genome. *Nature Genetics* 31:241–247.

Lamichhaney S, Berglund J, Almén MS, Maqbool K, Grabherr M, Martinez-Barrio A, Promerová M, Rubin CJ, Wang C, Zamani N, et al. 2015. Evolution of Darwin's finches and their beaks revealed by genome sequencing. *Nature* 518:371–375.

Langmead B, Salzberg SL. 2012. Fast gapped-read alignment with Bowtie 2. *Nature Methods* 9:357–359.

Lasne C, Sgrò CM, Connallon T. 2017. The Relative Contributions of the X Chromosome and Autosomes to Local Adaptation. *Genetics* 205:1285–1304.

Lester LJ, Selander RK. 1979. Population genetics of haplodiploid insects. *Genetics* 92:1329–1345.

Li H, Handsaker B, Wysoker A, Fennell T, Ruan J, Homer N, Marth G, Abecasis G, Durbin R. 2009. The Sequence Alignment/Map format and SAMtools. *Bioinformatics* 25:2078–2079.

Lifschytz E, Lindsley DL. 1972. The role of X-chromosome inactivation during spermatogenesis (Drosophila-allocycly-chromosome evolution-male sterility-dosage compensation). *Proceedings of the National Academy of Sciences of the United States of America* 69:182–186.

Lindstedt C, Huttunen H, Kakko M, Mappes J. 2011. Disengtangling the evolution of weak warning signals: High detection risk and low production costs of chemical defences in gregarious pine sawfly larvae. *Evolutionary Ecology* 25:1029–1046.

Linnen CR, Farrell BD. 2007. Mitonuclear discordance is caused by rampant mitochondrial introgression in Neodiprion (Hymenoptera: Diprionidae) sawflies. *Evolution* 61:1417–1438.

Linnen CR, Farrell BD. 2008. Comparison of methods for species-tree inference in the sawfly genus Neodiprion (Hymenoptera: Diprionidae). *Systematic Biology* 57:876–890.

Linnen CR, Farrell BD. 2010. A test of the sympatric host race formation hypothesis in Neodiprion (Hymenoptera: Diprionidae). *Proceedings of the Royal Society B: Biological Sciences* 277:3131–3138.

Linnen CR, Kingsley EP, Jensen JD, Hoekstra HE. 2009. On the origin and spread of an adaptive allele in deer mice. *Science* 325:1095–1098.

Linnen CR, O'Quin CT, Shackleford T, Sears CR, Lindstedt C. 2018. Genetic basis of body color and spotting pattern in redheaded pine sawfly larvae (Neodiprion lecontei). *Genetics* 209:291–305.

Lohmueller KE, Degenhardt JD, Keinan A. 2010. Sex-Averaged Recombination and Mutation Rates on the X Chromosome: A Comment on Labuda et al. *American Journal of Human Genetics* 86:978–980.

Malinsky M, Svardal H, Tyers AM, Miska EA, Genner MJ, Turner GF, Durbin R. 2018. Whole-genome sequences of Malawi cichlids reveal multiple radiations interconnected by gene flow. *Nature Ecology and Evolution* 2:1940–1955.

Mank JE, Vicoso B, Berlin S, Charlesworth B. 2010. Effective population size and the Faster-X effect: Empirical results and their interpretation. *Evolution* 64:663–674.

Martin M. 2011. Cutadapt removes adapter sequences from high-throughput sequencing reads | Martin | EMBnet.journal. *EMBnet.journal* 1:10–12.

Martin SH, Dasmahapatra KK, Nadeau NJ, Salazar C, Walters JR, Simpson F, Blaxter M, Manica A, Mallet J, Jiggins CD. 2013. Genome-wide evidence for speciation with gene flow in Heliconius butterflies. *Genome Research* 23:1817–1828.

Matthey-Doret R, Whitlock MC. 2019. Background selection and F_{ST}: Consequences for detecting local adaptation. *Molecular Ecology* 28:3902–3914.

Mcbride CS, Singer MC. 2010. Field studies reveal strong postmating isolation between ecologically divergent butterfly populations. *PLoS Biology* 8:e1000529.

Meiklejohn CD, Landeen EL, Gordon KE, Rzatkiewicz T, Kingan SB, Geneva AJ, Vedanayagam JP, Muirhead CA, Garrigan D, Stern DL, et al. 2018. Gene flow mediates the role of sex chromosome meiotic drive during complex speciation. *eLife* 7:e35468.

Meisel RP, Connallon T. 2013. The faster-X effect: Integrating theory and data. *Trends in Genetics* 29:537–544.

Mendez FL. 2017. Differences in the effective population sizes of males and females do not require differences in their distribution of offspring number. *Theoretical Population Biology* 114:19–28.

Messer PW, Petrov DA. 2013. Population genomics of rapid adaptation by soft selective sweeps. *Trends in Ecology and Evolution* 28:659–669.

Moran P. 1959. The Theory of Some Genetical Effects of Population Subdivision. *Australian Journal of Biological Sciences* 12:109.

Muirhead CA, Presgraves DC. 2016. Hybrid Incompatibilities, Local Adaptation, and the Genomic Distribution of Natural Introgression between Species. *The American Naturalist* 187:249–261.

Nagylaki T. 1996. The diffusion model for migration and selection in a dioecious population. *Journal of Mathematical Biology* 34:334–360.

Normark BB. 2003. The Evolution of Alternative Genetic Systems in Insects. *Annual Review of Entomology* 48:397–423.

Nosil P, Sandoval CP. 2008. Ecological niche dimensionality and the evolutionary diversification of stick insects. *PLoS ONE* 3:e1907.

Ohta T. 1973. Slightly Deleterious Mutant Substitutions in Evolution. *Nature* 246:96–98.

Orr HA, Betancourt AJ. 2001. Haldane's Sieve and Adaptation From the Standing Genetic Variation. *Genetics* 157:875–884.

Owen RE. 1986. Gene frequency dines at X-linked or haplodiploid loci. *Heredity* 57:209–219.

Owen RE. 1988. Selection at two sex-linked loci. *Heredity* 60:415–425.

Parker JD, Hedrick PW. 2000. Gene flow and selection balance in haplodiploid social insects. *Heredity* 85:530.

Patten MM. 2018. Selfish X chromosomes and speciation. *Molecular Ecology* 27:3772–3782.

Peter BM, Huerta-Sanchez E, Nielsen R. 2012. Distinguishing between Selective Sweeps from Standing Variation and from a De Novo Mutation. *PLoS Genetics* 8:e1003011.

Peterson BK, Weber JN, Kay EH, Fisher HS, Hoekstra HE. 2012. Double digest RADseq: An inexpensive method for de novo SNP discovery and genotyping in model and non-model species. *PLoS ONE* 7:e37135.

Petry D. 1983. The effect on neutral gene flow of selection at a linked locus. *Theoretical Population Biology* 23:300–313.

Pfenninger M, Patel S, Arias-Rodriguez L, Feldmeyer B, Riesch R, Plath M. 2015. Unique evolutionary trajectories in repeated adaptation to hydrogen sulphide-toxic habitats of a neotropical fish (*Poecilia mexicana*). *Molecular Ecology* 24:5446–5459.

Pinho C, Hey J. 2010. Divergence with Gene Flow: Models and Data. *Annual Review of Ecology, Evolution, and Systematics* 41:215–230.

Pouyet F, Aeschbacher S, Thiéry A, Excoffier L. 2018. Background selection and biased gene conversion affect more than 95% of the human genome and bias demographic inferences. *eLife* 7:e36317.

Presgraves DC. 2018. Evaluating genomic signatures of “the large X-effect” during complex speciation. *Molecular Ecology* 27:3822–3830.

R Core Team. 2020. R: A Language and Environment for Statistical Computing.

Rauf A, Benjamin DM. 1980. The biology of the white pine sawfly, Neodiprion pinetum (Hymenoptera: Diprionidae) in Wisconsin. *The Great Lakes Entomologist* 13:219–224.

Ravinet M, Faria R, Butlin RK, Galindo J, Bierne N, Rafajlović M, Noor MAF, Mehlig B, Westram AM. 2017. Interpreting the genomic landscape of speciation: a road map for finding barriers to gene flow. *Journal of Evolutionary Biology* 30:1450–1477.

Samuk K, Owens GL, Delmore KE, Miller SE, Rennison DJ, Schluter D. 2017. Gene flow and selection interact to promote adaptive divergence in regions of low recombination. *Molecular Ecology* 26:4378–4390.

Schweyen H, Rozenberg A, Leese F. 2014. Detection and Removal of PCR Duplicates in Population Genomic ddRAD Studies by Addition of a Degenerate Base Region (DBR) in Sequencing Adapters. *The Biological Bulletin* 227:146–160.

Seehausen O, Butlin RK, Keller I, Wagner CE, Boughman JW, Hohenlohe PA, Peichel CL, Saetre GP, Bank C, Brännström Å, et al. 2014. Genomics and the origin of species. *Nature Reviews Genetics* 15:176–192.

Slatkin M. 1991. Inbreeding coefficients and coalescence times. *Genetical Research* 58:167.

Sousa V, Hey J. 2013. Understanding the origin of species with genome-scale data: Modelling gene flow. *Nature Reviews Genetics* 14:404–414.

Tigano A, Friesen VL. 2016. Genomics of local adaptation with gene flow. *Molecular Ecology* 25:2144–2164.

Vertacnik K. 2020. Predicting patterns of gene family evolution in taxa with similar ecological niches. *Theses and Dissertations--Biology 67* [Internet]. Available from: https://uknowledge.uky.edu/biology_etds/67

Vertacnik KL, Linnen CR. 2015. Neodiprion lecontei genome assembly Nlec1.0. NCBI/GenBank.

Vicoso B, Charlesworth B. 2006. Evolution on the X chromosome: Unusual patterns and processes. *Nature Reviews Genetics* 7:645–653.

Vicoso B, Charlesworth B. 2009. Effective population size and the Faster-X effect: an extended model. *Evolution* 63:2413–2426.

Weir BS, Cockerham CC. 1984. Estimating F-statistics for the analysis of population structure. *Evolution*:1358–1370.

Wickham H. 2016. ggplot2: Elegant Graphics for Data Analysis. Springer-Verlag New York

Wilfert L, Gadau J, Schmid-Hempel P. 2007. Variation in genomic recombination rates among animal taxa and the case of social insects. *Heredity* 98:189–197.

Wolf JBW, Ellegren H. 2017. Making sense of genomic islands of differentiation in light of speciation. *Nature Reviews Genetics* 18:87–100.

Wood DE, Salzberg SL. 2014. Kraken: Ultrafast metagenomic sequence classification using exact alignments. *Genome Biology* 15:R46.

Wright AE, Harrison PW, Zimmer F, Montgomery SH, Pointer MA, Mank JE. 2015. Variation in promiscuity and sexual selection drives avian rate of Faster-Z evolution. *Molecular Ecology* 24:1218–1235.

Wright S. 1931. Evolution in Mendelian populations. *Genetics* 16:97.

Wright S. 1969. Evolution and the Genetics of Populations, Volume 2: Theory of Gene Frequencies, Wright. London: The University of Chicago Press

Yeaman S, Aeschbacher S, Bürger R. 2016. The evolution of genomic islands by increased establishment probability of linked alleles. *Molecular ecology* 25:2542–2558.

Yeaman S, Otto SP. 2011. Establishment and maintenance of adaptive genetic divergence under migration, selection, and drift. *Evolution* 65:2123–2129.

A. Fitness Model of Diploid Chromosomes

Fitness	AA	Aa	aa
Population 1	1	1+hs	1+s
Population 2	1+s	1+(1-h)s	1

Fitness Model of Haploid Chromosomes

Fitness	A	a
Population 1	1	1+s
Population 2	1+s	1

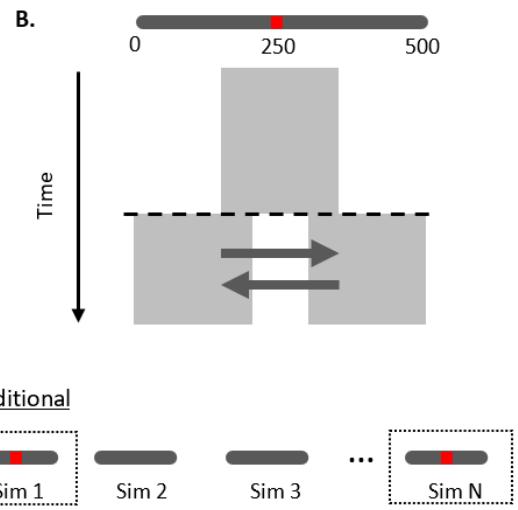

Figure 1. Overview of methodological approach. **A.** Fitness models for diploid chromosomes (autosomes and hemizygous chromosomes in females) and haploid chromosomes (hemizygous chromosome in males). Parallel dominance model where the fitness of heterozygotes depend on the dominance of allele *a*, which is assumed to be the same in both populations. Population 1 is the population where the derived allele is beneficial. **B.** Overview of stochastic simulations under an isolation-with-migration model. An ancestral population with an effective size of $2N_e$=1500 gene copies (i.e., hemizygous locus with 500 females and 500 males, and diploid locus with 375 females and 375 males) of a 500-kb chromosome (dark grey bar) evolves for 10,000 generations to reach mutation-drift equilibrium. This population then splits into two equally sized populations. A divergently selected site at position 250-kb (red line) with two alleles is introduced at the time of split, with an initial frequency q_0 of allele *a* in both populations. The populations evolve for T_{div}=2,000 generations experiencing symmetric migration at a constant rate. For each parameter combination, 1,000 simulations were run. **C.** The two approaches used to summarize simulation results. In the "all simulations" approach, we compute the mean F_{ST} across all simulations (i.e., accounting for cases where the derived allele *a* was lost due to drift). In the "conditional" approach, we compute the mean F_{ST} only across simulations where the derived allele *a* was retained.

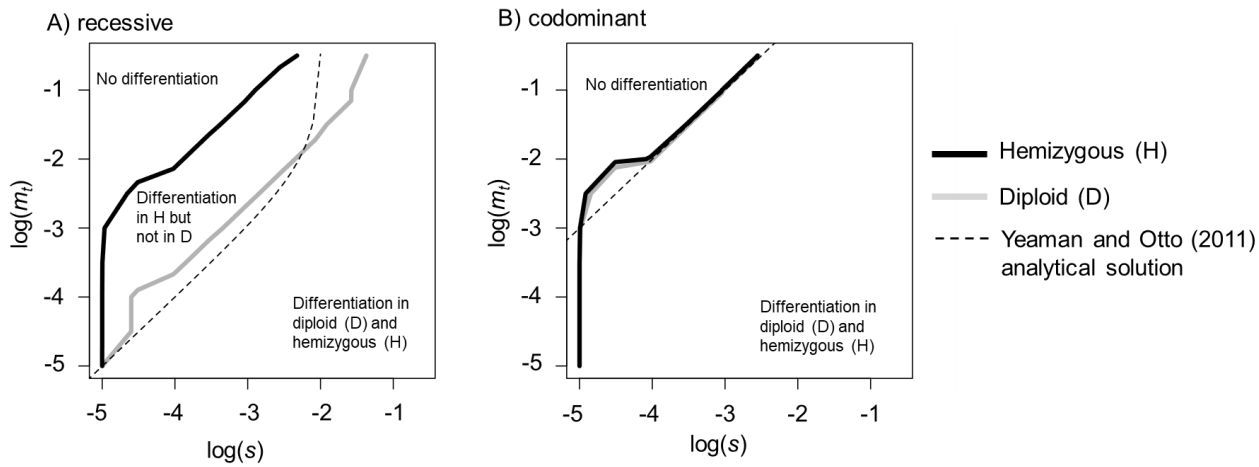

Figure 2. Migration threshold for a new mutation in hemizygous and diploid loci as a function of the selective coefficient (deterministic simulations). **A**. recessive, and **B**. codominant alleles. Solid lines indicate the migration threshold obtained with deterministic simulations defined as the region where $F_{ST}>10^{-10}$ at generation 10^5 for a new mutation (initial frequency $q=10^{-5}$). Dashed lines indicate the analytical solution of Yeaman and Otto (2011) for a diploid locus under a continent-island model. Migration thresholds (m_t) and selective coefficients (s) are reported in log10 scale.

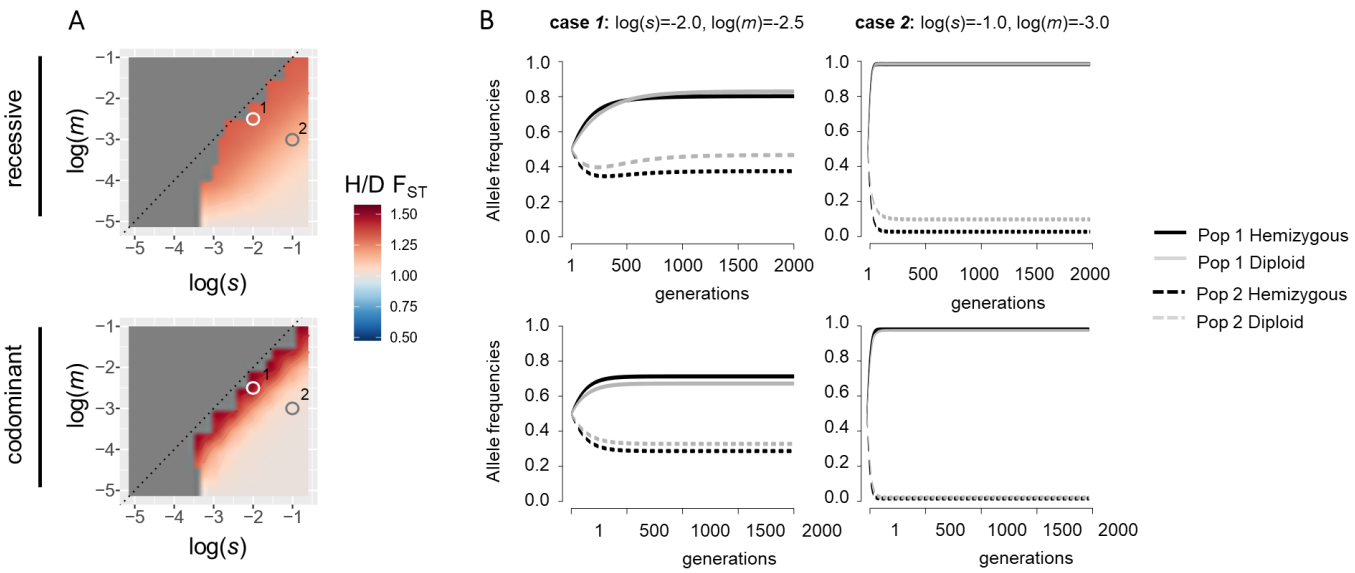

Figure 3. Faster-X adaptive differentiation at migration-selection equilibrium (deterministic simulations). A. Ratio of hemizygous to diploid (H/D) differentiation (F_{ST}) for recessive and codominant mutations with initial frequency q_0=0.50. Only regions where migration-selection equilibrium was found for both diploid and hemizygous are shown. Regions of the parameter space where equilibrium was not found after 10^5 generations are shown in gray. **B**. Allele frequency trajectories in populations 1 and 2 for hemizygous and diploid loci for two regions of the parameter space. For case *1*, both recessive and codominant mutations show faster-X differentiation, but the magnitude of the effect is larger for codominant mutations. For case *2*, only recessive mutations show faster-X differentiation. For these analyses, we focused on the highest starting allele frequency (q_0 = 0.5) because equilibrium differentiation levels were not affected by starting allele frequencies (Supplemental Figure S3) and this allele frequency had the most simulations that reached equilibrium (Supplemental Figure S1).

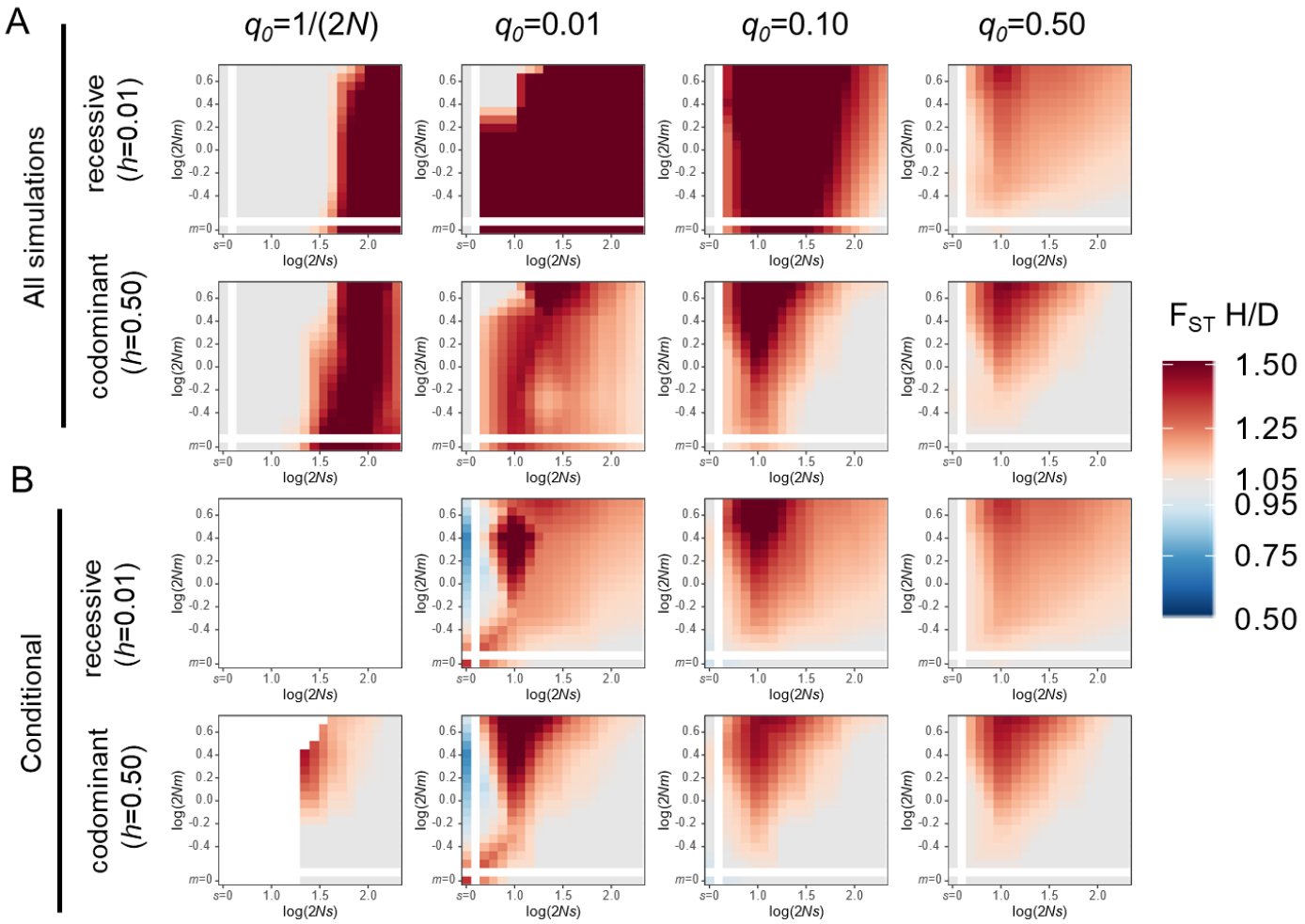

Figure 4. Faster-X adaptive differentiation at a locus under divergent selection (stochastic simulations). Ratio of hemizygous to diploid (H/D) differentiation (F_{ST}) for recessive and codominant mutations with different initial frequencies q_0. Results of average F_{ST} ratios **A**) across all 1000 simulations for each parameter combination; and **B**) conditional on simulations retaining the beneficial derived allele *a* in population 1. Scaled selection coefficient 2*Ns* (x-axis) and scaled migration rate as number of immigrants per generation 2*Nm* (y-axis) are represented in log10 scale. Note that *2Ns*=0 and *2Nm*=0 values are shown at *s*=0 and *m*=0. The heatmap F_{ST} H/D scale was truncated: values larger than 1.5 were assigned the same red color, and all values lower than 0.5 were assigned the same blue color. Heatmaps were obtained using a 2D barycentric interpolation of a grid of 7 selection x 4 migration rate parameter combinations. In B, for q_0=1/(2*N*) cases where there were less than 10 runs retained are shown as missing data in white.

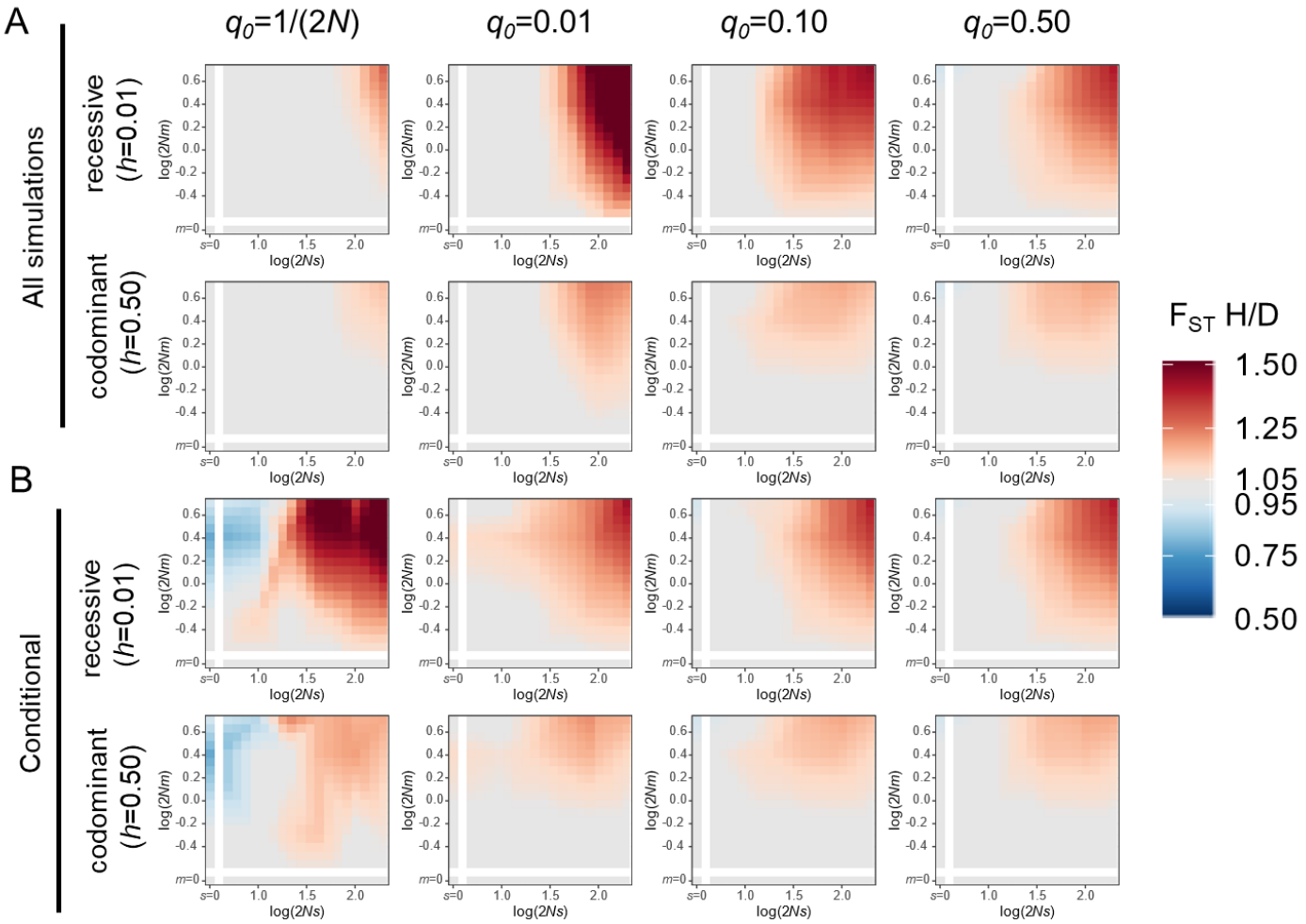

Figure 5. Faster-X adaptive differentiation at neutral sites linked to locus under divergent selection (stochastic simulations). Ratio of hemizygous to diploid (H/D) differentiation (F_{ST}) across 500Kb for a sample of 20 gene copies from each population, for recessive and codominant mutations with different initial frequencies q_0. Results of average F_{ST} ratios A) across all 1000 simulations for each parameter combination; and B) conditional on simulations retaining the beneficial derived allele *a* in population 1. Scaled selection coefficient 2*Ns* (x-axis) and scaled migration rate as number of immigrants per generation 2*Nm* (y-axis) are represented in log10 scale. Note that *2Ns*=0 and *2Nm*=0 values are shown at *s*=0 and *m*=0. The heatmap F_{ST} H/D scale was truncated: values larger than 1.5 were assigned the same red color, and all values lower than 0.5 were assigned the same blue color. Heatmaps were obtained using a 2D barycentric interpolation of 7 selection x 4 migration rate parameter combinations.

Figure 6 Faster-X adaptive differentiation at selected and linked sites (stochastic simulations). A. Ratio of hemizygous to diploid (H/D) differentiation (F_{ST}) at the selected site (top row) and at linked sites (bottom row), for recessive (left) and codominant (right) mutations with an initial frequency q_0=0.10. **B.** Allele trajectories at selected site in both populations (top row) and F_{ST} along the chromosome in non-overlapping 20Kb windows (bottom row), for recessive (left) and codominant (right) mutations for case 1 (2*Ns* = 10 and *2Nm* = 5; see panel A). **C.** Allele trajectories at selected site (top) and windowed F_{ST} (bottom), for recessive (left) and codominant (right) mutations for case 2 (2*Ns* = 200 and *2Nm* = 2.5; see panel A).

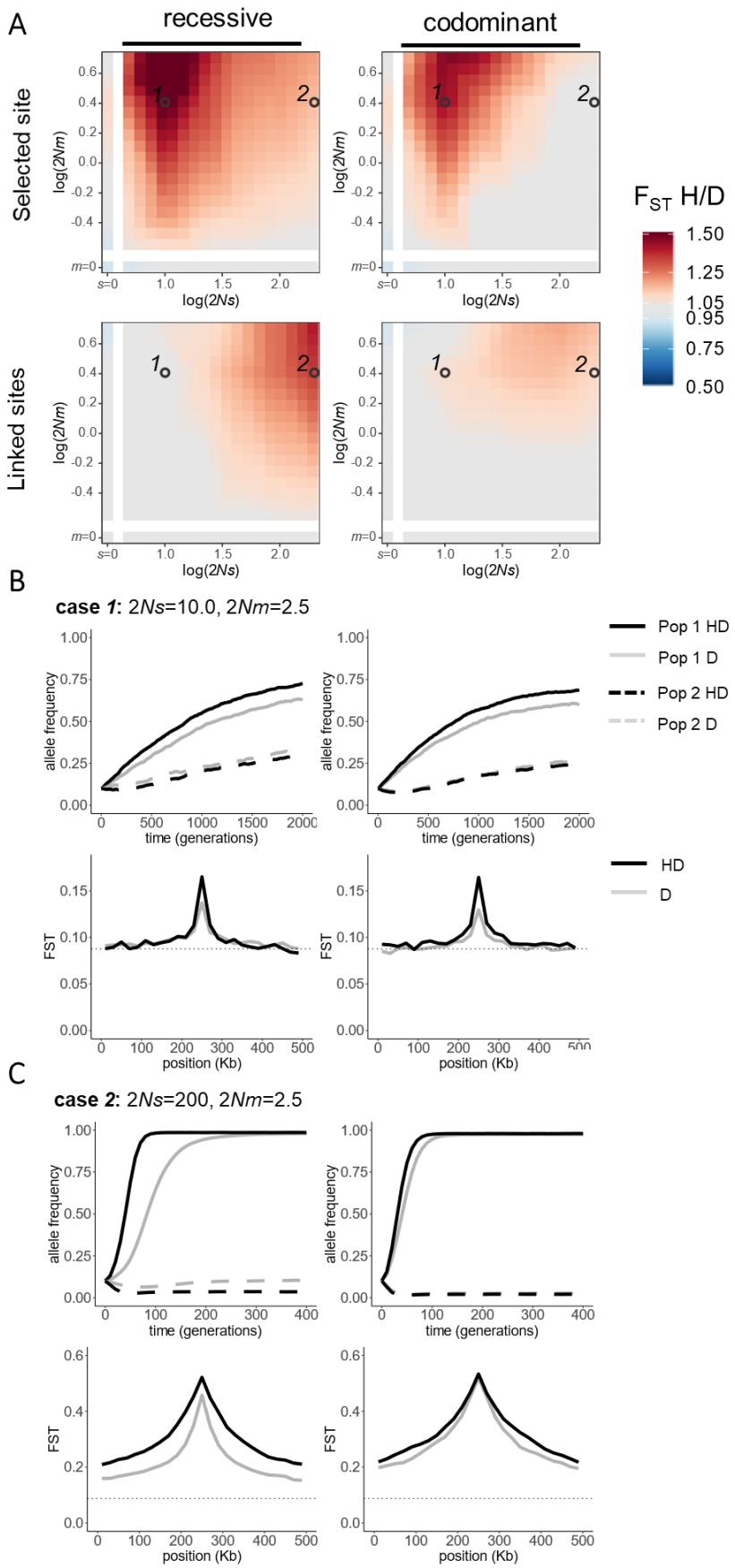

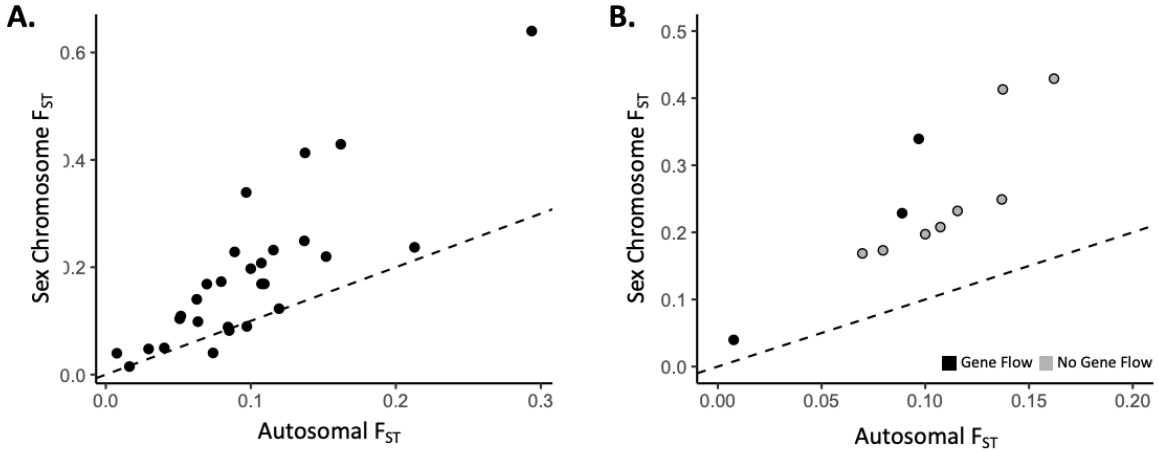

Figure 7. Meta-analysis of F_{ST} calculated from sex chromosomes and autosomes. **A.** Each point represents a taxon pair in Supplementary Table S6. F_{ST} values are the average of the per-site Weir and Cockerham's F_{ST} calculated from sex-chromosome and autosomal SNPs obtained from published datasets. The dashed line is equal F_{ST} in autosomes and sex chromosomes. Sex chromosomes tend to have higher F_{ST} than autosomes. **B.** F_{ST} values for taxon pairs from the genus *Heliconious* only (from Martin *et al.* 2013). Grey circles are taxon pairs without gene flow and black are experiencing gene flow.

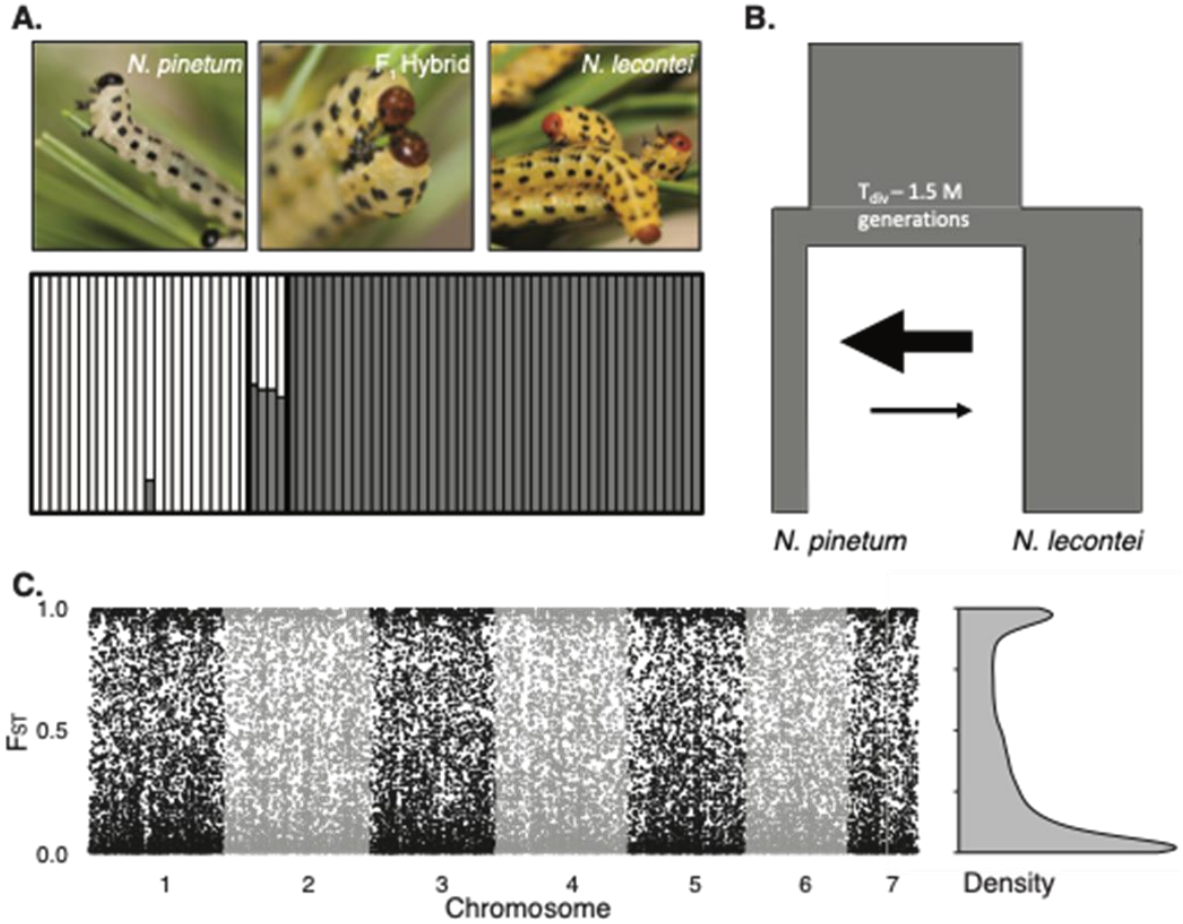

Figure 8. Population genomics of divergence and hybridization between *Neodiprion pinetum* and *N. lecontei*. A. Representative pictures of N. *pinetum*, *N. lecotnei*, and putative hybrid larvae above an Admixture plot of these populations. *N. pinetum* ancestry is in white and *N. lecontei* ancestry is in grey. Putative morphological hybrids are genetically admixed with approximately half of their ancestry coming from each species. **B.** *N. pinetum* and *N. lecontei* have diverged with continuous but asymmetric gene flow. Width of boxes is representative of population size and width of arrows is proportional to migration rate (see Supplementary Table S8 for parameter estimates). **C.** A Manhattan plot of per-site F_{ST} across the genome and a density plot of F_{ST} between *N. pinetum* and *N. lecontei.* F_{ST} is highly variable across the genome.

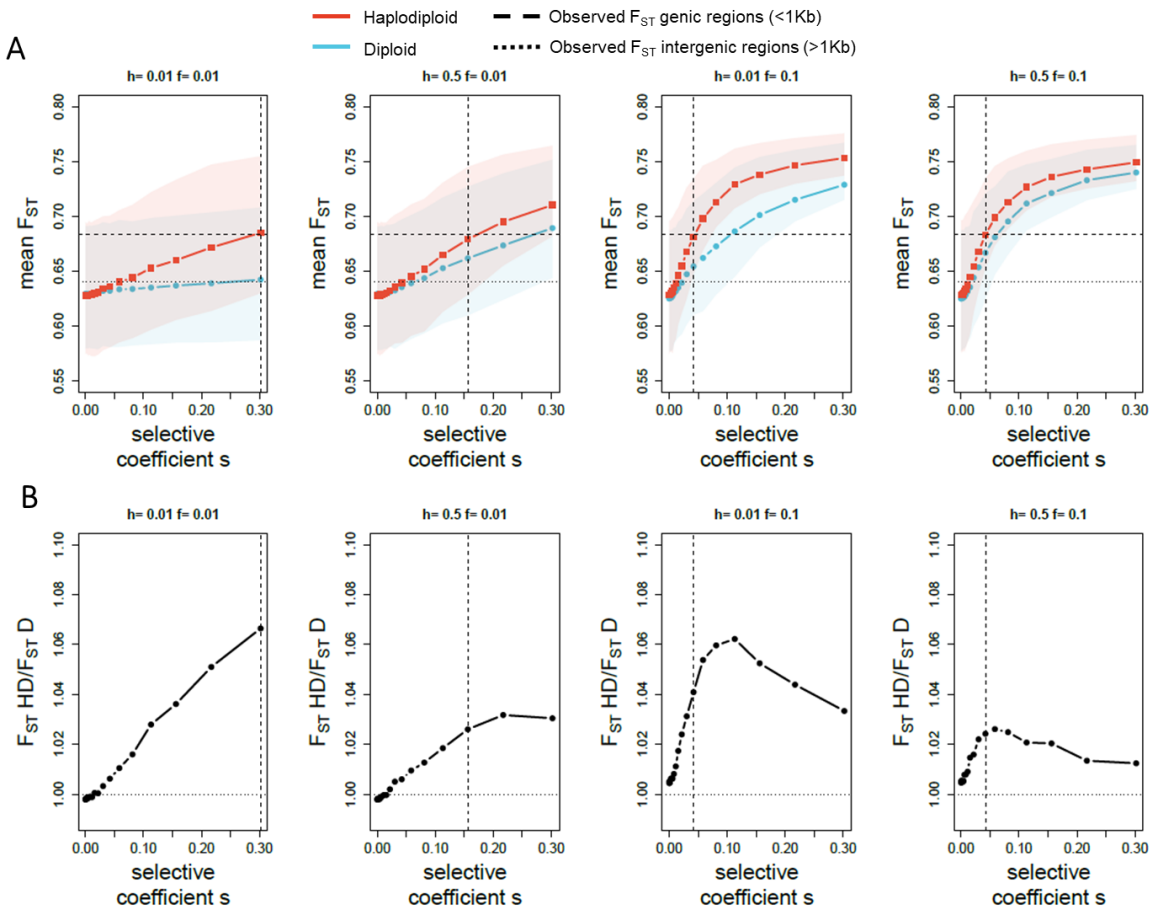

Figure 9. Effect of divergent selection on differentiation of *Neodiprion* sawflies, comparing haplodiploid and diploid scenarios. Results from stochastic simulations performed under the inferred demographic model for *N. pinetum* and *N. lecontei*, assuming a sex-ratio of 0.7 females and 0.3 males. A) Mean F_{ST} for diploid and haplodiploid as a function of selective coefficient for recessive (h=0.01) and codominant (h=0.50) mutations with different initial frequencies q_0=(0.01, 0.10). Results of mean F_{ST} ratios with shaded area indicating interquantile (0.25-0.75) range. Dotted horizontal line shows the observed mean F_{ST} at intergenic regions (>1Kb away from genes), dashed horizontal line indicates mean F_{ST} at genic regions (including 1Kb near genes). B) Ratio of mean F_{ST} for haplodiploid (HD) and diploid (D). F_{ST} values computed based on all 1000 simulations for each parameter combination. Vertical dashed line indicates the simulated mean haplodiploid F_{ST} that intercepts the observed F_{ST} at genic region.